Transition State Analysis of Thymidine Phosphorylase from *E. coli*

Mansoureh Rezaei

A Dissertation Presented to the Graduate Faculty of Middle Tennessee State University in Partial Fulfillment of the Requirements for the Doctor of Arts Degree

August, 2001

UMI Number: 3025235

UMI Microform 3025235

Bell & Howell Information and Learning Company
300 North Zeeb Road
P.O. Box 1346
Ann Arbor, MI 48106-1346

Transition State Analysis of Thymidine Phosphorylase from *E. coli*

Mansoureh Rezaei

Approved:

Paul C Kline

Dr. Paul C. Kline-Major Professor

Dr. Terrence A. Lee

Dr. Terrence A. Lee-Reader

Dr. William H. Ilsley-Reader

Jan Hayes

Dr. Jan Hayes-Reader

Dr. Earl Pearson-Chariman, Department of Chemistry

Dr. Donald L. Curry-Dean, College of Graduate Studies

This dissertation is dedicated to my mother and brother-in-law, whose love and memories I shall cherish as long as I live. They are my inspiration and strength.

ACKNOWLEDGEMENT

I would like to express my gratitude to Dr. Paul Kline for his mentoring and guidance through this project. I would like to thank Dr. William Ilsley for his computational chemistry expertise, and I am also indebted to Dr. Norma Dunlap for her invaluable assistance in organic syntheses. I would also like to thank the other members of my committee, Dr. Terrence Lee and Dr. Jan Hayes, for their advice, supervision, and encouragement. I would like to express my gratitude to many members of the faculty who have mentored and encouraged me, notably Dr. James Howard, Dr. Linda Wilson, and Dr. Gale Clark. I would like to thank Dr. Earl Pearson and Dr. Donald Curry for their continuous support.

I am also grateful to Mrs. Ann Smith, Mrs. Clara Todd, Mrs. Ann Nored, Miss Sara Nichols and Mr. Lewis Tigg for the support and encouragement I have received during my years at Middle Tennessee State University.

I would like to thank my family for their love and support. Finally, I am thankful to the Lord for not only giving me the answer to my prayer, he also shows me the way to a full life.

ABSTRACT

Thymidine phosphorylase (E.C. 2.4.2.4) (TP) is an enzyme involved in the reversible conversion of thymidine, deoxyuridine, and their analogs to their respective bases and 2-α-D-deoxyribose-1-phosphate. This enzyme is identical to an angiogenic factor, platelet-derived endothelial cell growth factor. TP is expressed at high levels in a wide variety of solid tumors and is known to promote the development of new blood vessels, which are fundamental to tumor growth and metastasis.

The transition state of thymidine phosphorylase has been characterized by kinetic isotope effects, bond-energy bond-order vibrational analysis, and molecular electrostatic potential surface and quantum chemical calculations. Kinetic isotope effects for arsenolysis were measured by liquid chromatography/mass spectrometry for [1′-^{2}H], [2′-^{2}H], [5′-^{2}H], [1′-^{13}C], [2′-^{13}C], and [1-^{15}N] uridine to provide experimental values of 1.144 ± 0.050, 0.959 ± 0.012, 0.988 ± 0.127, 1.013 ± 0.007, 0.995 ± 0.002, and 1.027 ± 0.046 respectively. These kinetic isotope effects were matched to a geometric transition state model selected by bond-energy bond-order vibrational analysis (BEBOVIB-IV program).

The transition state can be described as an S_N1 type reaction with oxocarbenium ion character with slight hyperconjugation existing between the C_2'-H_2' and C_1'-N_1 bonds, and C_4'-*endo* and C_3'-*exo* conformation of furanose ring due to protonation of O_2 in the uracil ring. Protonation of O_2 also assists departure of the uracil. From the BEBOVIB-IV calculations, the ^{13}C isotope effect predicts a bond order of 0.78 for C_1'-N_1, indicating an early transition state.

Inhibitor design for thymidine phosphorylase was attempted by incorporating features of the transition state.

TABLE OF CONTENTS

LIST OF TABLES

TABLE PAGE

LIST OF FIGURES

LIST OF EQUATIONS

CHAPTER ONE

INTRODUCTION

Thymidine phosphorylase (E.C. 2.4.2.4) from *Escherichia coli* is used as a catalyst in the syntheses of purine and pyrimidine 2'-deoxyribose nucleosides. This enzyme is one of the pyrimidine nucleoside phosphorylases that operate in the salvage pathway (1). Pyrimidine nucleoside phosphorylase (PYNP) catalyzes the reversible phosphorolysis of thymidine, deoxyuridine and their analogs to their respective bases and 2-α-D-deoxyribose-1-phosphate. This enzyme also catalyzes the transfer of deoxyribose from one deoxynucleoside to another base to form a second deoxynucleoside (Figure 1) (1,2). In lower organisms PYNP accepts both thymidine and uridine, whereas mammalian and other higher organisms have two separate PYNP enzymes, one specific for thymidine (thymidine phosphorylase EC 2.4.2.4) and one specific for uridine (uridine phosphorylase EC 2.4.2.3)(1). These phosphorylases exhibit considerable variation in physical properties, substrate specificity and mechanism even though they catalyze the same fundamental chemical reaction.

Figure 1: Enzymatic reaction of thymidine phosphorylase.

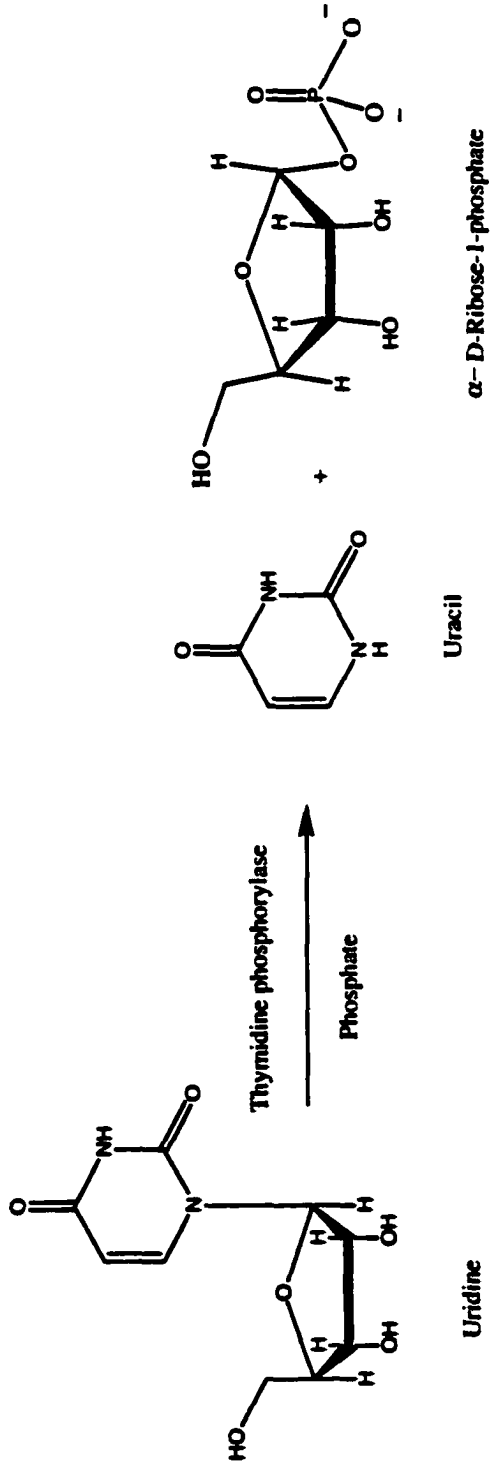

Pyrmidine nucleoside phosphorylases from *B. Sterarothermophilus*, *Haemophilus influenzae* and *E. coli* have 40% sequence identity to human thymidine phosphorylase and do not differentiate between uridine and thymidine. However, this enzyme apparently has no relationship with the human uridine phosphorylase (<20% sequence identity) (3).

Thymidine phosphorylase has been of interest due to its potential as a drug target in several chemotherapeutic strategies. Additional interest has surfaced with the recent findings that the sequence of human TP is identical to that of platelet-derived endothelial cell-growth factor. The fact that a single peptide (TP) functions both as an enzyme in an important metabolic pathway and as a growth factor for both endothelial cells and neurons makes this an exciting protein to study (4). Existence of multifunction proteins refutes the idea of one gene-one protein-one function (5). The multiple functions of such "moonlighting proteins" add another dimension to cellular complexity and benefit cells in several ways. After the sequence of complete genomes becomes available, the functions of the encoded proteins and how all these proteins come together to make a living cell will be determined. Many protein

functions can be inferred from the known functions of homologous proteins, but the existence of multifunctional proteins complicates such interpretation (5). For example, phosphoglucose isomerase (E.C. 5.3.1.9), is an enzyme in glycolysis and is also found moonlighting outside the cells as a nerve growth factor.

Any changes in cellular concentration of a ligand, substrate, cofactor or product, may cause changes in the function of a moonlighting protein. For instance, the same protein can perform two different functions in two different locations within the cell (5,6). Thymidine phosphorylase has different functions inside and outside the cell (5,6). In the cell cytoplasm, thymidine phosphorylase catalyzes the phosphorylation of thymidine, deoxyuridine and their analogues to the base and 2-deoxyribose-1-phosphate. In the extra-cellular fluid, it is platelet-derived endothelial cell growth factor, which stimulates endothelial cell growth and chemotaxis.

Thymidine phosphorylase was first purified and characterized as an enzyme involved in nucleic acid homeostasis. This enzyme has been purified from a variety of mammalian tissues, as well as several bacterial sources. Thymidine phosphorylase was first described almost 45 years

ago, and purified in the mid-1970s from both *Escherichia coli* and *Salmonella* (7). Thymidine phosphorylase (Figures 2 and 3) consists of two identical subunits with a molecular mass of 110 kDa (8,9) with a K_m of 0.38 mM for thymidine and 0.98 mM for phosphate (9). In *Escherichia coli* thymidine phosphorylase, the homodimer is reported to be 90 kDa (9).

Detailed structural information on this enzyme has been obtained from the crystal structure (10). The three-dimensional structure of thymidine phosphorylase from *Escherichia coli* has been determined at 2.8 Å resolution using multiple-isomorphous replacement techniques. The amino acid sequence deduced from the *deoA* DNA sequence has also been reported (10). Thymidine phosphorylase exists in the crystal as an S-shaped dimer in which the subunits are related by a crystallographic 2-fold axis (10). Each subunit is composed of a small α-helical domain of six helices and a large α/β domain. The α/β domain includes a six-stranded mixed β-sheet and a four-stranded antiparallel β-sheet (10). Three loops connect α and α/β domains. These loops act as hinges that allow the domains to move as rigid bodies.

Figure 2. Ribbon view of thymidine phosphorylase. α/β domain is red, the α domain is blue, and the three hinges are green.

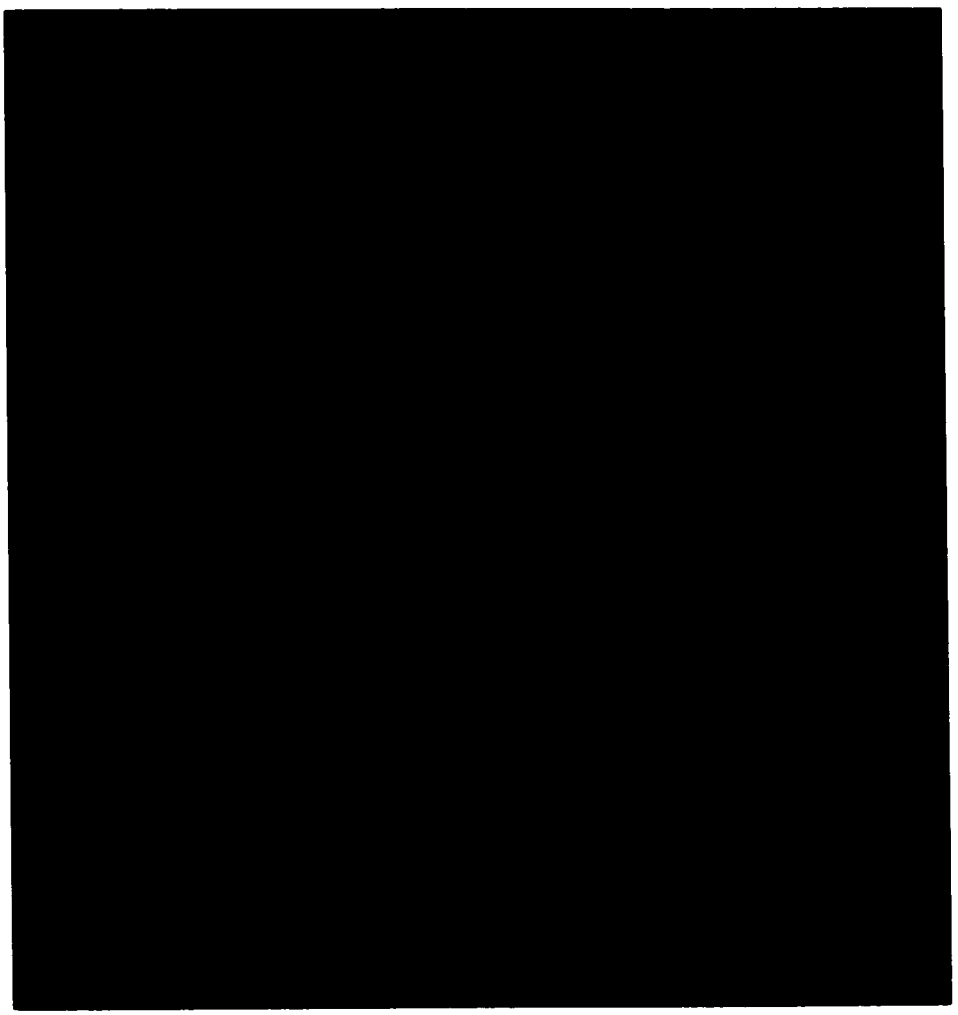

Figure 3. Cylinder view of thymidine phosphorylase. α/β domain is red, the α domain is blue, and the three hinges are green.

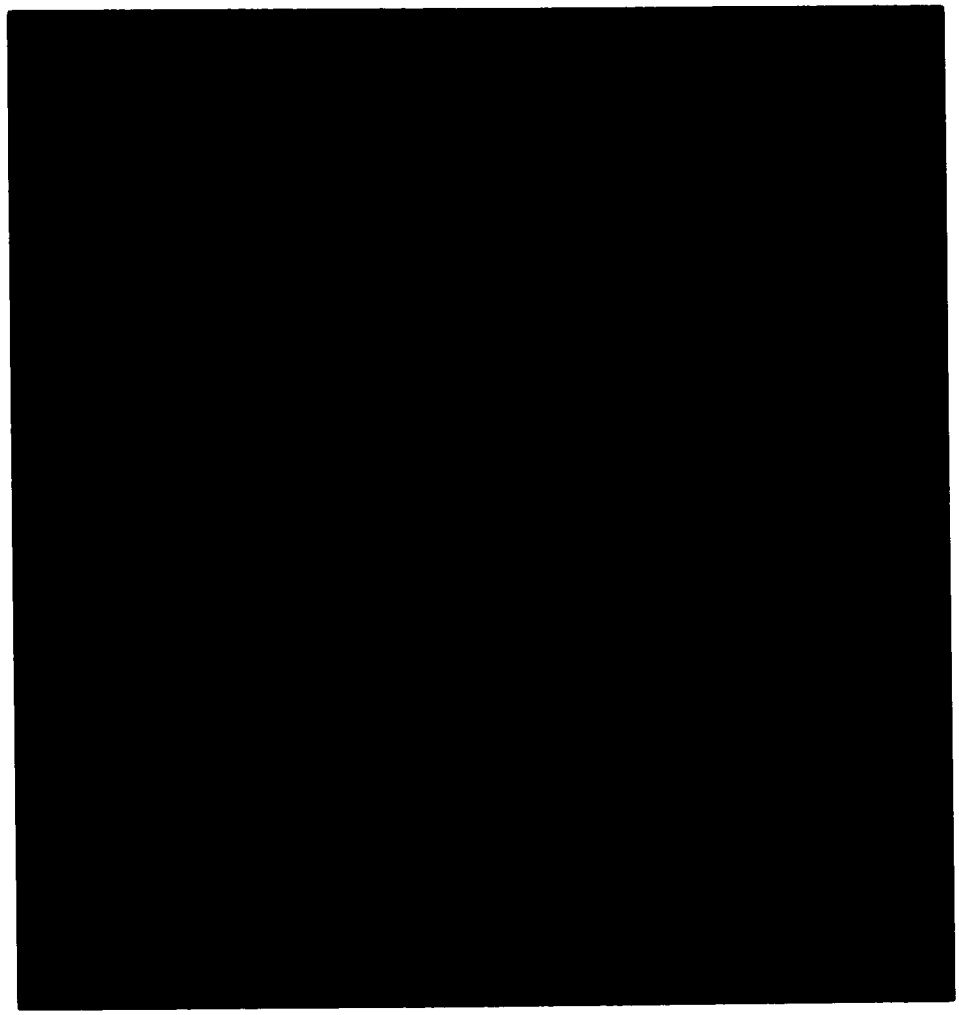

The active site was identified by difference Fourier analyses of the binding of thymine and thymidine and lies in a cleft between the small and large domains. Analysis of the base-binding site has implicated Arg-168, Ser-188, Lys-187 and Tyr-165 as the important residues in binding the pyrimidine base (10). Arg-168 on helix 9 is within hydrogen bonding distance of the carbonyl oxygen at position four of the nucleoside. The position of Arg-168 in the pyrimdine-binding site is such that the binding of deoxycytidine or any other nucleoside analogues with the hydrogen bond donor at C_4 would be distinctly unfavorable. A similar role is played by Lys-244 in human purine nucleoside phosphorylase (10) which is specific for 6-oxopurines and will not accept adenine nucleosides. As mentioned before, thymidine phosphorylase is capable of interacting with 2'-deoxynucleosides as well (11).

In the thymidine phosphorylase crystal structure, the 2'-deoxyribose moiety of thymidine is directed toward the sulfate/phosphate-binding site thereby bringing the sugar in close proximity to the loop containing residues 113-123 (12). The phosphate binding site is located in the α/β domain at the carboxyl terminal end of β-sheet A between

strands β_1A and β_2A (12). Residues from β_1A, β_2A and H_6 that are important in phosphate binding include Lys-81, Ser-83, Lys-108, Ser-110 and Thy-120 (12,13). Nucleoside binds in the β-conformation with a dihedral angle of the gylcosidic bond (O_4'-C_1'-N_1-C_2) of 165°, which is classified as (+) antiperplanar according to the Klyne and Prelog convention (14). The ribose moiety shows a C_4'-*endo* sugar pucker that is similar to several purine nucleosides bound to purine nucleoside phosphorylase. This C_4'-*endo* puckering decreases the dihedral angle of O_4'-C_1'-N_1-C_2 which makes the pyrimidine nucleoside assume an unusual high energy conformation that would likely put strain on the glycosidic bond. Glycosidic bond strain due to a high-energy nucleoside conformation is consistent with the catalytic mechanism proposed for the phosphorolysis of purine nucleosides (12).

The effect of substrate and product on thymidine phosphorylase activity suggests that it has evolved as a catabolic enzyme (15). Ittzsch et al. (15,16) showed that thymidine phosphorylase has several thymine-binding sites. When these sites are occupied, the enzyme is inhibited. Inhibition by end products is a common control mechanism;

however, it is most unusual for an enzyme to be inhibited by its substrate. Thymidine and phosphate co-operatively enhance thymidine phosphorylase activity. This is consistent with these being substrates. Again, one can postulate that this control mechanism would only evolve if thymidine were usually the substrate and not the product. The catabolic reaction is also responsible for the angiogenic activity (11).

Recently, a number of studies have demonstrated that thymidine phosphorylase is up regulated in human colon cancer and that this over-expression correlates with the formation of new blood vessels (17). The formation of new blood vessels from the existing vasculature is called angiogenesis. Angiogenesis is rare in the healthy adult, occurring only during wound healing, the female reproductive cycle and in regions that have become inadequately perfused due to an increased metabolic load (18,4). Angiogenesis is an essential component of solid-tumor growth and the progression of chronic inflammatory disease such as rheumatoid arthritis and psoriasis. The recognition that thymidine phosphorylase plays a role in angiognesis originated in 1987 with the purification of an endothelial growth factor from platelets (19). The factor

was found to be a chemoattractant for endothelial cell growth factor (PD-ECGF). PD-ECGF/TP does not stimulate the growth of endothelial cells and has no hydrophobic signal sequence (20). The exact mechanism of angiogenesis by PD-ECGF/TP is unknown. Thymidine phosphorylase shows angiogenic activity *in vivo* and its enzymatic activity is indispensable for its angiogenic effect. Among the products of thymidine degradation by thymidine phosphorylase, 2-deoxy-α-D-ribose, a dephosphorylated product derived from 2-deoxy-α-D-ribose-1-phosphate, showed chemotactic activity *in vitro* and angiogenic activity *in vivo* (19). These results suggest that TP phosphorolysis products may stimulate chemotaxis of endothelial and possibly other cells, causing angiogensis (19,20). Thymidine phosphorylase is elevated in many solid tumors and in chronically inflamed tissues, both known areas of active angiogenesis (20,21).

By 1992, experimental evidence showed that human platelet-derived endothelial cell growth factor and *Esherichia coli* thymidine phosphorylase are almost identical (16). Human platelet-derived endothelial cell growth factor apparently undergoes post-translational

maturation, whereby 10 and 4 amino acids are removed from the amino and carboxyl termini respectively (15). Mature platelet-derived endothelial cell growth factor has a 22 amino acid N-terminal extension with respect to the *Escherichia coli* thymidine phosphorylase sequence. The sequences show a 40% identity calculated over the 438 common amino acid positions. The conclusion drawn from this was the likelihood that thymidine phosphorylase in *Escherchia coli* and human thymidine phosphorylase shared a common genetic ancestor and contained the same overall tertiary fold (3). Based on studies with bacterial thymidine phosphorylase, characteristics of a pyrimidine-binding site for humans have been proposed, although very few specific and potent inhibitors have been identified, such as 7-deazaxanthine (7DX) and 6-amino-5-bromouracil (22,23).

The activity of thymidine phosphorylase has been reported to increase in several types of malignant tumors. As mentioned before, experimental evidence has shown that thymidine phosphorylase is identical to platelet-derived endothelial cell growth factor, and that thymidine phosphorylase has angiogenic activity (20,21). When tumors reach a size of a few millimeters, new capillaries

penetrate them, allowing rapid growth. These new vessels facilitate the entry of tumor cells into the vasculature and their subsequent metastasis, so that angiogenesis correlates with the probability of metastases (24,25). For example, thymidine phosphorylase expression in human gastric carcinomas showed a significant correlation between the proportion of metastasis and the microvessel density. Microvessels were counted in the tumors of 158 patients whose tumors were completely removed surgically. The correlation between angiogenesis and thymidine phosphorylase expression was more frequent in gastric carcinomas than in normal tissues (26). Among 158 patients, 67 (43.4%) showed a direct correlation between angiogenesis and thymidine phosphorylase. The correlation in the control group was only 7.6%. Similar findings have been reported in regards to breast, prostate, colorectal, and lung carcinoma (27,28,29). These studies suggest that thymidine phosphorylase expression is correlated with microvessel density. Since angiogenesis is central to the pathological conditions of tumor growth, rheumatoid arthritis, diabetic retinopathy, and psoriases (19,27,30), a detailed understanding of the molecular action of

thymidine phosphorylase (platelet-derived endothelial cell growth factor) must be accomplished.

In spite of the enormous effort on understanding of bacteria, mice, and human thymidine phophorylase and its role in carcinomas, a clinically effective anti-thymidine phosphorylase agent has not been identified. The inter-species and intra-species differences in substrate specificities and activities between human and animal thymidine phosphorylase may have an important impact on the validity of attempts to introduce inhibitors of these enzymes into the clinic or on drawing conclusions about the metabolism and the chemotherapeutic use of pyrimidine analogs in humans, based on studies in other living organism. Although, analogues such as 5'-deoxy-5-fluororuidine (5'-DFUR), 2'-deoxy-5-fluorouridine (FdUrd) and 5-iodo-2'-deoxyuridine inhibit both mammalian and bacterial thymidine phosphorylase, very few potent inhibitors have been identified (31,32). There are tremendous obstacles to be faced in developing a clinically effective drug. One new technique is the combinatorial libraries method. This method was introduced in 1991 and allows the synthesis of large numbers of compounds at one time. These can then be tested for activity and all

promising compounds are isolated. But this method is a very time-consuming process. Each analogue has to be synthesized and tested for activity. This process is essentially one of trial and error.

Rational drug design method is another approach which chemists have used recently (33,34). In this approach specific enzymes will be targeted for inhibition. In order to "rationally" design an inhibitor of an enzyme, the exact structure of the enzyme's active site must be determined. The active site can be considered a pocket or hole where the enzyme's substrate or target molecule is processed (34,35). In the "rational drug design" approach the inhibitor is designed from the ground up based on the coordinates or structure of the active site. These inhibitors are very precisely designed so that they bind to very specific molecular sites within the active site. A good inhibitor will remain in the active site for a long time, while a poor inhibitor will fall out and allow the enzyme's natural substrate to reenter.

The two basic "rational drug design" approaches are: 1) determining the active site structure which relies heavily on the use of computers and X-ray crystallography of the target protein and 2) determining the transition

state structure using kinetic analysis (33,34). In order to determine the active site architecture by X-ray crystallography, the enzyme has to be isolated in large amounts and highly purified. After the enzyme is purified to the extent that a crystal can be formed, the crystallized enzyme is analyzed by X-ray crystallography to determine its structure (33).

X-ray crystallography is unable to provide accurate information on the transition state of the substrate since inter atomic distances of a few tenths of an angstrom result in large differences in transition state reactivity and these distances are well below the resolution limits of X-ray crystallography (33). However, x-ray crystallography is able to give information on the stable complexes, which are next to the transition state on the reaction.

There is a second approach to "rational drug design". This approach consists of determining the transition state structure of an enzyme catalyzed reaction through kinetic analysis. Kinetic isotope effects provide detailed information concerning geometry bond angle, charge, bond length, and other conformational properties about the transition-state structure of an enzyme. Ultimately this information can be used to design and synthesize potential

transition state analogs that should be potent inhibitors of the enzyme.

The transition states of a number of different enzymes have been determined including AMP nucleosidase, AMP deaminase and S-adenosylmethionine synthetase among others (36-39). Among the most detailed is that of nucleoside hydrolase. The transition state of nucleoside hydrolase has been characterized by using a family of kinetic isotope effects. Electrostatic modeling along with kinetic isotope effects was used to develop transition state analogues. Inhibitor design for nucleoside hydrolase was attempted by incorporating features of the experimentally determined transition state into a family of inhibitors with single and multiple features of the transition state. The electrostatically similar phenyliminoribitol binds 12,000 times tighter than substrate and nitrophenylriboamidrazone binds 190,000 times tighter than substrate (40). Nitrophenylriboamidrazone was found to be the best nucleoside hydrolase inhibitor due to its geometry, charge and hydrogen-bonding features that mimic the transition-state. Nitrophenyriboamidrazone has an equilibrium dissociation constant, k^*_i, 15-fold lower than that previously reported for 1'-phenylaminoribitol (2 vs 30 nM)

(40). Application of KIEs has also been successfully employed in designing tight-binding inhibitors of AMP nucleosidase (41,42). KIEs have been used to characterize the mechanism of S-adenosylmethionine syntheses as well (41).

When the reaction rate constant of a chemical reaction is changed by the substitution of an isotope in a reacting molecule, the change is called a kinetic or rate isotope effect (KIE) (43). For instance, if both hydrogen atoms in a water molecule are substituted by deuterium atoms, the rates of some of the reactions of water molecules are reduced by 50% or more (43). The substitution of a carbon isotope causes a much smaller isotope effect than does the substitution of a hydrogen isotope (43). This smaller isotope effect is to be expected, since the masses of ^{12}C and ^{14}C differ by less than 17%, whereas the mass of a deuterium atom is twice that of a hydrogen atom. Rate isotope effects are expressed conveniently as ratios of specific reaction rate constants. The ratio most often used is k/k^*, in which k is the reaction rate constant of normal molecule, and k^* is that of the isotopic substituted molecules (43).

An isotope effect (k/k*) arises from the difference in zero-point energies between the labeled and unlabeled transition state minus the corresponding values for the ground state (43). The zero-point energy is related to the difference in bonding, for the two isotopic species of reactants in the ground state and transition state. The magnitude of the zero-point energy depends on the degree of change of bonding to the isotopic atom in going from the ground state to the transition state. If no change in bonding occurs, there is no KIE. If bonding to the isotopic atom decreases, the expected isotope effects are greater than unity, (that is, the lighter isotope reacts more rapidly than the heavier isotope). An inverse KIE is observed if the "heavy" substrate has a faster conversion to product. Isotope effects have been defined as primary and secondary (44). Primary isotope effects are those resulting from isotopic substitution at a site where at least one bond is being made or broken. Bond breakage is generally attributed to be a rate-determining transition state. Secondary isotope effects result from the change in the force constant of the isotope in proceeding from the ground state to the transition state of the reaction (41).

The most generally applicable method for measuring KIEs is the competitive method, using a mixture of two labeled substrates. One labeled substrate contains a label at an isotopically sensitive position while the other contains a different isotopic label at a remote position. (40). In this method the isotopic composition of the substrate or product is measured as a function of the extent of the reaction. If the labeling isotope is radioactive, the specific activity of the starting material or product is measured and the isotope ratio determined to approximately $\pm$ 0.1%. If the labeling isotope is stable, isotope-ratio mass spectrometry has been used for the measurement of isotopic composition (43). But when a high molecular weight organic compound containing carbon-13 is to be analyzed by mass spectrometry the compound is usually degraded to a simpler gaseous carbon-containing compound, which is inserted in a mass spectrometer for determination of the $^{13}C/^{12}C$ ratio (43).

While radioactive substrates provide accurate KIEs, the use of them leads to several difficulties. Substrates must be synthesized with radioactive labels in specific positions which sometimes generate significant waste compounds. In addition, regulations and the expense for

disposal are rapidly increasing. The ease of disposal and increased safety are the advantages of using stable over radioactive isotopes. A disadvantage of the use of stable isotopes is that the kinetic isotope effects for ^{13}C and ^{2}H are inherently smaller than those of ^{14}C and ^{3}H.

Mass spectrometry has evolved as an important technique for the measurement of stable isotopes such as ^{13}C, ^{2}H and ^{15}N. The combination of gas or liquid chromatography and mass spectrometry provides a rapid, sensitive, and efficient method for the direct analysis of stable carbon isotopes individually, in volatile organic compounds, and in chemically complex samples. While it has been used extensively, gas chromatography analysis of nucleosides is frequently constrained by the necessity to prepare derivatives of sufficient volatility and stability for the vapor phase separation.

Nucleosides can be directly analyzed by LC/MS without going through derivatization. The elimination of the need for chemical modification of the sample by derivatization is a major characteristic of any of the interfaces between liquid chromatography and mass spectrometer. This elimination becomes a substantial practical advantage that permits the mass spectrometric analysis of a nonvolatile,

thermally labile, and/or precharged molecule. On the other hand, these interfaces must be able to accommodate the greatly increased molecular flow rates associated with liquid chromatography relative to gas chromatography (45).

Qualitative work using LC/MS requires no major changes from other MS techniques. However, in contrast to GC/MS, LC/MS spectra have a greater number of background ions due to the mobile phases and buffers present (45). Removal of the solvent ions is best accomplished through the use of a background subtraction process in the data reduction programs of most LC/MS systems. Additionally, LC/MS generally requires more sample for the analysis as compared to GC/MS due to some losses in sample transport and ion formation process (45).

SIM (selective ion monitoring) and Scan are two ways of operating the mass spectrometer in both GC/MS and LC/MS. When high sensitivity is needed for trace organic compounds, the mass spectrometer has a special mode (SIM) which can provide additional sensitivity for detection of these trace compounds while maintaining high specificity. The SIM technique allows the user to select a set of ions unique to the target compound and to monitor only those ions rather than scanning through the entire spectrum. By

spending more time on each selective ion and less time on scanning the entire spectrum, the sensitivity is increased by factors of 10 to 100. This technique is used for quantitative analysis and is able to detect picograms ($\cong 1.66 \times 10^{12}$ amu) of drugs and pollutants in complex matrices (45).

Following the determination of the experimental isotope effect using the gas chromatography/mass spectrometer or liquid chromatography/mass spectrometer, the values were matched to a geometric transition state model selected by bond-energy bond-order vibrational analysis (BEBOVIB-IV) program available from the Quantum Chemistry Program Exchange (46). The bond-energy bond-order vibrational approach to calculate kinetic isotope effects has been reviewed by Sims and Lewis based on empirical relationships for use in assigning force constants for angle bends and torsional coordinates given certain structural information. The program calculates a kinetic isotope effect given a ground state structure and proposed transition state structure. The ground state structure is often based upon the crystal structure of the starting material. The transition state structure was varied systematically until

the calculated isotope effects matched the experimentally determined kinetic isotope effects. A combination of kinetic isotope effects using the gas or liquid chromatography/mass spectrometer and BEBOVIB-IV can deduce novel transition state conformation (38,39,46).

CAHPTER TWO

MATERIALS AND METHODS

MATERIALS AND REAGENTS:

Uridine, uracil, and silica gel for flash chromatography, and thymidine phosphorylase were purchased from Sigma. α-D-ribofuranose-1,3,5-tribenzoate, β-D-ribofuranose-1-acetyl-2,3,5-tribenzoate, benzoyl chloride, hexamethyldisilazane (HMDS), trimethylsilyl trifluoromethanesufonate, methanolic ammonia, dicyclohexylcarbodiimide (DCC), deuterated acetic acid, bromoacetic acid, bromine, platinum oxide, 5% palladium on barium sulfate, $NaBD_4$, $Na_2S_2O_3 \cdot 5H_2O$, and $CeCl_3 \cdot 7H_2O$ were purchased from Aldrich. [1'-^{2}H] and [2'-^{13}C] uridine were synthesized previously according to the procedure of Kline and Serianni (51). Labeled [1'-^{13}C] uridine was a gift from OMICRON Biochemical.

EQUIPMENT AND INSTRUMENTATION:

Isotope composition of samples was determined using a Hewlett-Packard (HP) 1100 capillary column liquid chromatograph, interfaced to a HP 1100 mass spectrometer and HP G1315A diode array detector. Data collection and

instrumentation control were performed using a HP 1100 MS chemstation.

UV-visible light measurements were obtained using a Hewlett-Packard (HP) diode array spectrophotometer 8452 (DAD).

NMR data for all samples were collected on a 200 MHZ Bruker AC 200 NMR spectrometer.

SYNTHESIS OF [2'-^{2}H] URIDINE:

Tri-O-benzoyl-2-ketoribofuranose:(50)

1.00 g (2.0 mmol) of α-D-ribofuranose-1,3,5-tribenzoate was added to a solution of Dess Martin periodinane (1.375 g, 3.243 mmol) in 10 mL of CH_2Cl_2 at 0 °C. The mixture was allowed to warm to room temperature and stirred for 14 h (hour). The solvent was evaporated under reduced pressure and the residue triturated with 20 mL of diethyl ether. Following filtration through a pad of $MgSO_4$, the organic solvent was stirred with an equal volume of $Na_2S_2O_3 \cdot 5H_2O$ (2.5 g) in 20 mL of saturated $NaHCO_3$ until the organic layer became clear (~10 min.). The organic layer was separated, washed with brine, and dried over $MgSO_4$ prior to removal of the solvent *in vacuo*. α-D ketofuranose-1,3,5-tribenzoate (0.75 g, 74%) was precipitated from a

mixture of ether and hexane (2 mL ether, 0.5 mL hexane). The oxidized sample "ketone" was analyzed by NMR Bruker AC 200. ^1H NMR ($CDCl_3$) δ: 8.20-7.99 (5H,m), 7.70-7.34 (10H,m), 6.12 (1H,s,H_1), 5.79 (1H,d,H_3), 5.2-4.90 (1H,m,H_4), 4.80-4.70 (1H,dd,H_5), 4.62-4.50 (1H,dd,H_5).

α-D-1,3,5-Tri-O-benzoyl-2-deutero ribofuranose:(50)

0.402 g of dried $CeCl_3 \cdot 7H_2O$ and 0.75 g of α-D-Ketofuranose-1,3,5-tribenzoate in 8.9 mL of THF were stirred under argon for 30 min. at room temperature. 0.136 g of $NaBD_4$ was added in one portion, and the mixture was stirred for 1 h at room temperature. The reaction was quenched by the slow addition of 0.80 mL of AcOH-d. After being stirred for 3 h, the reaction was diluted with 35.8 mL of diethyl ether and washed with H_2O. The organic layer was dried over $MgSO_4$ and concentrated under reduced pressure. Flash chromatography of the residue (EtOAc/Hexane 3/7) yielded α-D-2-deuteroribofuranose-1,3,5-tribenzoate (0.50 g, 66%). ^1H NMR ($CDCl_3$) δ 8.20-8.02 (5H,m), 7.70-7.35 (9H,m), 6.70 (1H,s,H_1), 5.60 (1H,d,H_3), 4.78-4.73 (1H,m,H_4), 4.68-4.64 (2H,m,H_5).

α-D-1,2,3,5-Tetra-O-benzoyl-2-deuteroribofuranose: (50)

Dried benzoyl chloride (2.0 mL, 16. mmol) was added via syringe to α-D-2-deuteroribofuranose-1,3,5-tribenzoate (0.5 g, 1 mmol) in pyridine (8.0 mL). After being stirred for 12 h, the reaction was quenched via addition of H_2O (8.0 mL), immediately followed by slow addition of $NaHCO_3$ (2.713 g). The mixture was extracted with diethyl ether (129.0 mL) and the organic layer dried and concentrated as described above. Flash chromatography of the residue (EtOAc/Hexane 3/7) yielded α-D-2-deuteroribofuranose-1,2,3,5-tetrabenzoate (0.47 g, 94%). ^1H NMR ($CDCl_3$) δ 8.35-8.02 (6H,m), 7.90-7.84 (2H,m), 7.59-7.25 (12H,m), 6.98 (1H,s,H_1), 5.96-5.92 (1H,d,H_3), 4.97-4.91 (1H,m,H_4), 4.84-4.60 (2H,dd*dd,H_5).

Condensation of protected sugar with Uracil: (51)

A reflux apparatus was assembled with 0.0876 g (0.782 mmol) of uracil in the reaction flask. After the apparatus was purged with argon, 3.60 mL of HMDS was added. The suspension was refluxed under argon until the base completely dissolved (~2h). Excess HMDS was removed by distillation at atmospheric pressure, leaving clear syrup. The last trace of HMDS was removed by vacuum distillation at 50 °C. Then 0.228 g (0.390 mmol) of α-D-2-

deuteroribofuranose-1,2,3,5-tetrabenzoate was dissolved in 7.0 mL of anhydrous CH_2Cl_2 and 0.20 mL of trimethylsilyl trifluoromethanesulfonate. This mixture was added to the reflux apparatus containing the silylated base, and the reaction mixture was refluxed under argon for 4 h. The formation of nucleoside was monitored by TLC (70/30 of EtOAc/Hexane).

After the condensation reaction was completed, the reaction mixture was cooled to room temperature and diluted with 14.0 mL of methylene chloride. The solution was extracted with 14.0 mL of ice-cold saturated aqueous sodium bicarbonate and the organic phase was dried over anhydrous sodium sulfate. The solvent was removed under reduced pressure at 30 °C. Flash chromatography of the residue (EtOAc/Hexane 40/60) yielded 0.24 g (21%) of protected [2'-^{2}H] uridine. ^{1}H NMR ($CDCl_3$) δ 8.20-8.01 (6H,m) 7.62-7.25 (16H,m), 6.30 (1H,d,H'_1), 5.91-5.82 (1H,d,H_5), 5.65-5.57 (1H,d,H'_3), 4.90-4.60 (1H,m,H'_4)4.18-4.05.(2H,m,H'_5)

Removal of benzoyl group: (51)

The benzoyl protecting groups were removed with methanolic ammonia. Uridine was dissolved in methanolic ammonia and incubated at 25 °C for 16 h. The solvent was

removed under reduced pressure at 30 °C and the residue dissolved in 4 mL of distilled water. The aqueous solution was extracted three times with 10 mL of chloroform and 10 mL of diethyl ether. The aqueous phase was concentrated by vacuum distillation at 30 °C and the syrup applied to a 2 cm * 21 cm column containing reverse phase silica gel bonded C_{18}. The effluent was monitored continuously at 264 nm. Uridine was eluted with the distilled water and solvent was removed under reduced pressure at 30 °C. 0.069 (28%) g of labeled uridine obtained. ^1H NMR (D_2O)δ 7.7 (1H,d,H_6), 5.3-5.67 (1H,d,H'_1), 5.66-5.63 (1H,d,H_5), 4.05-3.86 (2H,m,H'_3,H'_4), 3.76-3.50 (2H,m,H'_5).

SYNTHESIS OF [5'-^{2}H] URIDINE: (52)

A solution of 0.1 g (2.0 mmol) of 2'-3'-O-isopropylideneuridine and 0.2204 g (1.068 mmol) of dicyclohexylcarbodiimide in 0.8 mL of dry methyl sulfoxide was treated with 7.0 μL of dichloroacetic acid. The mixture was stirred, under dry conditions, for 1.5 h. The formation of product was monitored by TLC (1/10 CH_3OH/CH_2Cl_2). The reaction was terminated by addition of 0.0416 g of oxalic acid dihydrate in 1 mL of ethanol.

The precipitated solids were removed by filtration and washed twice with 2 mL ethanol. The acidic filtrate was carefully neutralized (pH 7.5) with a few drops of 4 M aqueous sodium hydroxide, and 0.006 g (0.1 mmol) of sodium borohydride-d_4 was added, portion-wise, with stirring, to the solution. After 10-15 min., the excess reagent was decomposed by addition of glacial acetic acid (final pH 6.5), and the solvent was removed under reduced pressure at 45 °C.

The crude product was extracted with 15 mL of hot chloroform. The solvent was evaporated under reduced pressure at 50 °C, and crude product was purified by flash chromatography (CH_3OH/CH_2Cl_2 1/10) (0.050 g, 50%). ^1H NMR ($CDCl_3$)δ 7.70 (1H,d,H_6),5.80 (1H,d,H'_1), 5.72-5.66 (1H,d,H_5), 4.95-4.85 (2H,m,H'_2,H'_3), 4.32-4.25 (1H,m,H'_4), 3.86-3.73 (1H,dd,H'_5), 1.60-1.30 (6H,2s,$2CH_3$).

Deprotection of [5'-^{2}H] isopropylidene uridine:

To the purified [5'-^{2}H] isopropylidine uridine, 4 mL HCl was added and incubated for 10 min. at 80 °C. The reaction mixture was neutralized with a few drops of 4 M NaOH. The solvent was removed under reduced pressure at

45 °C. The residue was purified by flash chromatography on reverse phase silica gel bonded C_{18}. The effluent was monitored continuously at 264 nm. The main UV-absorbing peak was pooled and lyophilized (0.050 g, 30%). ^1H NMR (D_2O) δ 7.70-7.63 (1H,d,H_6), 5.74-5.70 (1H,d,H'_1), 5.69 (1H,d,H_5), 4.20-4.10 (1H,dd,H'_3), 4.05-3.98 (1H,dd,H'_2), 3.95-3.88 (1H,dd,H'_4), 3.70-3.55 (1H,dd,H'_5).

SYNTHESIS OF [1-^{15}N] URIDINE:(53)

Bromoacetic acid (2.8 g, 20 mmol) in water (6mL) was carefully neutralized with 1.5 g (11 mmol) of anhydrous potassium carbonate, followed by slow addition of 1.05 g (15.1 mmol) of [^{15}N] potassium cyanide in water (5 mL). The mixture was allowed to stir at ambient temperature (22 °C) for 15 min. and heated to 60 °C (oil bath) for 25 min. The solution was cooled to 10 °C and acidified by the addition of 3.70 mL of an 6N hydrochloric acid. The product was extracted with diethyl ether in a continuous liquid-liquid extractor for 72 h, the ether extract was dried over anhydrous sodium sulfate, and solvent was removed to afford 0.75 g (8.7 mmol, 58%) of [1-^{15}N] cyanoacetic acid. NMR analysis indicated that no bromoacetic acid remained.

[1-^{15}N]-β-Alanine Hydrochloride:

To a solution of 0.75 g (8.6 mmol) of [1-^{15}N] cyanoacetic acid in water (25 mL) was added 6 mL of concentrated hydrochloric acid. The mixture was hydrogenated at 70 psi over platinum oxide (0.25 g) and the theoretical uptake of hydrogen was realized after 40 h. The catalyst was filtered off and washed with water (4×15 mL). The filtrate and washings were combined and water was removed at reduced pressure giving 1.0 g of a pale yellow solid (not all water had been removed).

[1-^{15}N]-β-Alanine:

The hygroscopic [1-^{15}N]-β-alanine hydrochloride from the reduction was dissolved in deionized water (5 mL) and applied to 25 mL of IR-40 resin [previously washed successively with 1% aqueous hydrochloric acid (250 mL), 1% aqueous sodium hydroxide, and finally deionized water (500 mL)]. The free amino acid was eluted from the column with deionized water (250 mL). Removal of water under reduced pressure gave 0.70 g (90%) of a pale yellow solid.

[1-^{15}N]-5,6-Dihydrouracil:

To a solution of 0.70 g (8.6 mmol) of [1-^{15}N]-β-alanine

in water (20 mL) was added 1.6 g (20 mmol) of potassium cyanate dissolved in 20 mL of water. The solution was slowly evaporated to dryness by heating in an oil bath (100 °C) under a stream of nitrogen. A syrupy residue, consisting of the potassium salt of [1-^{15}N]-β-ureidopropionic acid, solidified on standing. This potassium salt was acidified with 40 mL of 6 N hydrochloric acid, the solution was evaporated to dryness, and the residue was heated at 170 °C for 30 min. The solid residue was thoroughly washed with 5-mL portions of water until all of the potassium chloride had been removed (negative silver nitrate test), and the residue was dried over phosphorus pentoxide to afford 0.395 g of [1-^{15}N]-5,6-dihydrouracil. The water washes were combined and continuously extracted with ether for 72 h to afford a further 0.1 g (100%) of crude [1-^{15}N]-5,6-dihydrouracil.

(Bis-O-trimethylsilyl) [1-^{15}N] Uracil:

A magnetically stirred suspension of 0.495 g (4.30 mmol) of [1-^{15}N]-5,6-dihydrouracil in 10 mL glacial acetic was heated in an oil bath (maintained at 105 °C) until the entire solid had dissolved. The flask was fitted with a dropping funnel and protected with an efficient dry-ice

condenser. The dropping funnel was charged with 9.3 g (58 mmol) of bromine dissolved in 5 mL glacial acetic acid and the solution was added slowly to the solution of dihydrouracil at 105 °C at such a rate to just maintain the bromine color. After all of the bromine color had been dissipated (3-4 h), the solvent was removed on a rotary evaporator under reduced pressure to afford a white solid. ^{1}H NMR analysis confirmed the absence of any starting dihydrouracil and showed the solid to contain 5-bromodihydrouracil and 5,5-dibromodihydrouracil in approximately equal proportions. The solid mixture was heated at 210 °C (oil bath, preheated) for 25 min. under a stream of nitrogen to assist in the removal of the hydrogen bromide generated during the elimination, giving a mixture of [1-^{15}N] uracil and [1-^{15}N]-5-bromouracil. The mixture was dissolved by gentle heating in 100 mL of 50% aqueous ethanol and the resulting solution was hydrogenated over 1.0 g of 5% palladium on barium sulfate for 5 h. The solution was heated to boiling and the catalyst was removed by filtration and washed with hot water (4x15 mL). The combined filtrate and washing were evaporated to dryness under reduced pressure to afford crude [1-^{15}N] uracil (0.220 g) as a pale yellow solid. Figure 7 illustrates an MS chromatogram of

[1-^{15}N] uracil.

Condensation of protected sugar with [1-^{15}N] Uracil:

The reaction vessel was assembled with 0.220 g (1.94 mmol) of [1-^{15}N] uracil in the reaction flask. After the vessel was purged with argon, 2.0 mL of HMDS and 1 mL of DMSO was added. The suspension was refluxed under argon for 4 h. Excess HMDS was removed by distillation at atmospheric pressure. Then 0.084 g (0.17 mmol) of β-D-ribofuranose-1-acetyl-2,3,5-tribenzoate was dissolved in 2.0 mL of anhydrous CH_2Cl_2 and 0.10 mL of trimethylsilyl trifluoromethanesulfonate. This mixture was added to the reaction vessel containing silylated base, and the reaction mixture was refluxed under argon for 16 h. The formation of nucleoside was monitored with TLC (70/30 of EtOAc/Hexane).

After the condensation reaction was complete, the reaction mixture was cooled to room temperature and diluted with 6.0 mL of methylene chloride. The solution was extracted with 6.0 mL of ice-cold saturated aqueous sodium bicarbonate and the organic phase was dried over anhydrous sodium sulfate. The solvent was removed under reduced pressure at 30 °C. Flash chromatography of the residue (EtOAc/Hexane 40/60) yielded 0.010 (11%)g of protected [1-^{15}N] uridine.

Removal of benzoyl group:

The benzoyl protecting groups were removed with methanolic ammonia. 2,3,5-Tri-O-benzoyl[1-^{15}N]uridine was dissolved in methanolic ammonia and incubated at 25 °C for 16 h. The solvent was removed under reduced pressure at 30 °C and the residue dissolved in 4 mL of distilled water. The aqueous solution was extracted three times with 10 mL of chloroform and 10 mL of diethyl ether. The aqueous phase was concentrated by vacuum distillation at 30 °C and the syrup applied to a 2 cm × 21 cm column containing reverse phase silica gel bonded C_{18}. The effluent was monitored continuously at 264 nm by UV spectrophotometer. Uridine was eluted with distilled water and solvent was removed under reduced pressure at 30 °C. 0.0040 g (40%) of labeled uridine was obtained. ^{1}H NMR (D_2O) δ 7.7 (1H,dd,H_6), 5.3-5.67 (1H,dd,H'_1), 5.66-5.63 (1H,dd,H_5), 4.05-3.86 (2H,m,H'_3,H'_4), 3.76-3.50 (2H,m,H'_5).

MEASUREMET OF KINETIC ISOTOPE EFFECTS:

Kinetic isotope effects were measured by determining the ratio of stable isotopes in the product using liquid chromatography/mass spectrometry. For each KIE experiment,

two reactions were run, one to 20-30% completion and the other to 100% completion. The 100% reaction provides the control ratio of $^{1}H/^{2}H$, $^{12}C/^{13}C$ or $^{14}N/^{15}N$ and the 20-30% reaction provides the $^{1}H/^{2}H$, $^{12}C/^{13}C$ or $^{14}N/^{15}N$ ratio changed by the presence of a kinetic isotope effect. Reaction mixture preparation consists of the following steps:

1. 200 µL of labeled (10 mM) and unlabeled uridine (10 mM) were combined and diluted with 800 µL of 50 mM sodium arsenate @ pH 7.4 and 800 µL of distilled water to yield 1 mM nucleoside concentration.
2. The reaction mixture was divided into two equal volumes. Reaction was initiated by addition of 1 µL of thymidine phosphorylase from *Escherichia coli* @ pH 7.4 (partial hydrolysis), and the other by addition of 10 µL thymidine phosphorylase from *Escherichia coli* @ pH 7.4 (control).
3. The reaction progress was monitored by LC/MS with a mobile phase of 97.5% deionized H_2O and 2.5% CH_3OH on a 150 mm × 2.0 mm C_{18} column at 0.4 mL/min with detection at 260 nm. The partial hydrolysis reaction mixture was stopped at approximately 30% completion by addition of 100 µL 1M HCl. The control reaction mixture containing the

concentrated enzyme was allowed to proceed to 100% completion at which time 100 μL of 1 M HCl was added. The ratio of partial hydrolysis ($^{1}H/^{2}H$, $^{12}C/^{13}C$ or $^{14}N/^{15}N$) to complete hydrolysis ($^{1}H/^{2}H$, $^{12}C/^{13}C$ or $^{14}N/^{15}N$) was determined by LC/MS.

LIQUID CHROMATOGRAPHY/MASS SPECTROMETRY:

Uridine, uracil, and ribose were separated on a Hewlett Packard (HP) capillary column liquid chromatograph interfaced with an API mass spectrometer (LC/MS). The injection volume was 1 μL, the flow rate was 0.4 mL/min with a mobile phase of 97.5% water and 2.5% methanol. The mass spectrometer detector (electrospray) was operated in a positive ion mode with gas temperature of 350 °C, drying gas flow rate of 13.0 L/min and a nebulizer pressure of 25 psig. The spectral collection range was from 190 nm to 400 nm.

Samples were analyzed under SIM conditions. For each m/z monitored, extracted ion chromatograms (EIC) were prepared and integrated. This procedure minimized potential errors in the enrichment calculations by minimization of the random contribution of the baseline to the ions monitored. Isotope enrichments, E, based on the integrated area of the extracted ion chromatograms, were calculated using the following formula:

$$E = [I(P+1)/(Ip + I(P+1)](100) \quad (1)$$

where I_P and $I_{(P+1)}$ are the intensities for the unlabeled and labeled samples respectively.

CALIBRATION CURVE PREPARATION FOR LC/MS:

Calibration curves for [1-^{2}H] and [1-^{13}C] ribose were constructed to relate observed enrichment to actual enrichment. Appropriate volumes of labeled and unlabeled 10 mM ribose solutions were combined to yield 12 1 mM solutions containing 0%, 5%, 10%, 20%, 30%, 40%, 50%, 60%, 70%, 80%, 90% and 100% label. Suitable volumes of water and $NaHArSO_4$ (Sodium Arsenate) stock solutions were added to each solution to yield to 1 mM concentration. Figures 8 and 9 show calibration curves for [1-^{13}C] and [1-^{2}H] respectively.

CALCULATION OF KINETIC ISOTOPE EFFECTS:

Kinetic isotope effects were determined by the measurement of the relative rates of hydrolysis of the nucleoside containing a light (natural abundance) or heavy atom in a given position. Kinetic isotope effects were calculated using the following equation:

$$\text{Observed isotope effect} = \frac{\dfrac{\text{isotope representing natural isotope}}{\text{isotope representing heavy isotope}}\ (10\text{-}30\%\ \text{hydrolysis})}{\dfrac{\text{isotope representing natural isotope}}{\text{isotope representing heavy isotope}}\ (100\%\ \text{hydrolysis})} \qquad (2)$$

Observed kinetic isotope effects were corrected to %0 hydrolysis using the following equation:

$$\text{Actual isotope effect} = \frac{\ln\left[1-(\text{fraction hydrolyzed})(\text{observed isotope effect})\right]}{\ln(1-\text{fraction hydrolyzed})} \qquad (3)$$

Fraction hydrolyzed is based on the integration of the area obtained from UV spectrum.

TRANSITION-STATE MODELING:

Bond-energy bond-order vibration analysis (BEBOVIB-IV program) was used to match experimental kinetic isotope effects of [1'-^{13}C], [2'-^{13}C], [1'-^{2}H], [2'-^{2}H], [5'-^{2}H] and [1-^{15}N] to proposed transition state.

Initial transition states were modeled based on the structural information from the X-ray structure of *E. coli* TP and also the proposed catalytic mechanism of thymidine phosphorylase. All of the models were built in Spartan and energy minimized. The refinement of the models was carried out in Spartan 5 and Gaussian 98W. The Restricted Hartree-

Fock (RHF) method with 3-21G* and 6-31G* basis set, was used for optimizing of the models. The transition state was searched as follow:

1 The second oxygen in the uracil ring was protonated,

2 A Geometry optimization performed using Gaussian 98W, and

3 The Cartesian coordinates obtained from optimization transferred to BEBVIB-IV.

Protonation of O_4 and hydrogen bonding to O_4 and O_2 of the uridine were other hypothetical transition state models considered. Their geometries were optimized using the same procedure noted above. The Cartesian coordinates obtained from all the hypothetical transition state structures were imported into the BEVOVIB-IV program to calculate KIE.

In order to make the modeling process feasible, the large number of internal coordinates (bond length, bond angles, and torsional angles) was condensed into a few parameters. Atoms are located by R (distance from the origin), ϕ (angle measured from the positive X axis) and θ (angle measured from the positive Z axis). θ and ϕ values obtained from the refinement of the uridine were then assigned bond orders. For the first bond defined and assigned, a bond order of one was given. For succeeding

bonds of the same type, the single-bond distance assigned for the first bond was used, but the bond order for the true distance was adjusted using Pauling's equation:

$$R_{(n)} = R^{(1)} - 0.3 \ln (n) \qquad (4)$$

Force constants for the various vibrational modes were derived from reported values (48,49,50). Due to limitation on the maximum number of atoms employed in a BEBOVIB model, only the relevant atoms (20) for the transition state structure were used, (49,50). The ground state structure for the truncated uridine used for vibrational analysis of the transition state was in the C_3'-*endo* conformation established by X-ray crystallography. This structure contained ribosyl and imidazole ring moieties, but omitted the hydroxylic hydrogen atoms, 3', 4', and one of the 5'hydrogen (Figure 11).

All BEBOVIB analyses were obtained using an IRIX system Silicon Graphics 02 workstation with a GDM-17e21 Monitor.

CHAPTER THREE

DISCUSSION

Transition state analogs are potent enzyme inhibitors which make them objects of considerable interest in drug design and discovery. In transition state theory, the enzyme is more suited to make favorable contacts with the transition state of the substrate compared with the substrate in its normal conformation (ground state). From this a compound that resembles the transition state in geometry and electronic structure will bind more tightly to an enzyme than will the substrate. There has been considerable interest in the search for such "transition-state analogs", since these would help to confirm ideas about transition states of reactions. To construct a transition state analog, the transition state structure for the enzymatic reaction must be determined. A powerful technique for determining transition states is analysis of kinetic isotope effects. Transition state analysis using kinetic isotope effects requires:

1. synthesis of substrates with heavy atoms at positions which may experience altered vibrational force-fields at the transition state
2. measurement of heavy-atom kinetic isotope effects,
3. correction for enzymatic steps that suppress kinetic isotope effects
4. use of Bond-Energy Bond-Order Vibrational analysis (BEBOVIB) to propose transition state structure
5. calculation of charge distribution on the transition state (34).

SYNTHESES OF LABELED NUCLEOSIDES:

[2'-^{2}H] Uridine was synthesized according to the procedure of Cook and Greenberg (49) (Figure 4). The reaction sequence started with oxidation of α-D-ribofuranose-1,3,5-tribenzoate followed by reduction with sodium borodeuteride, condensation with uracil and removal of protecting groups with methanolic ammonia. The overall chemical yield was 28%. An analysis of the product by LC/MS indicated the incorporation of the label was 50%.

The first step in the synthesis of [5'-^{2}H] was the oxidation of the hydroxylmethyl group to the aldehyde.

Figure 4: Synthesis of [2'-^{2}H] uridine.

a:Dess-Martin Periodinane; b:$NaBD_4$; c:Benzoyl chloride/pyridine d:Trimethylsilyl trifluoromethanesulfonate/uracil (B=Uracil); e:NH_3, Saturated MeOH

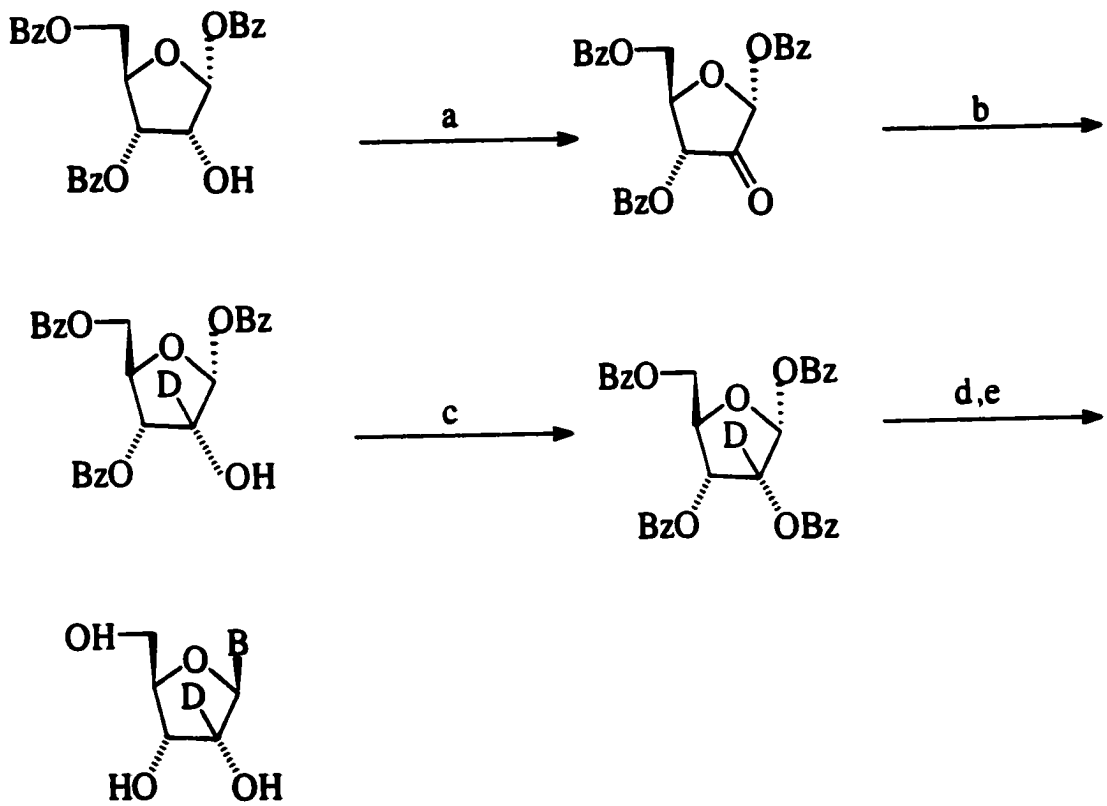

Oxidation of 2',3'-O-isopropylideneuridine to uridine-5'-aldehyde was accomplished using the Pfitzner-Moffatt reagent (N,N'-dicyclohexylcarbodiimide-dimethyl sulfoxide) (52). The overall yield was 30% and analysis of product by LC/MS indicated 30% labeled was incorporated (Figure 5).

[1-^{15}N] Uridine was synthesized through a multi step synthesis starting with bromoacetic acid using the procedure of Robert and Poulter (Figure 6) (53). The overall yield was 11%. An analysis of product by LC/MS confirmed the incorporation of the label was 100%.

CALIBRATION CURVES:

Calibration curves for [1-^{13}C] and [1-^{2}H] ribose were constructed to relate observed enrichment to actual enrichment (Figure 8 and 9). They were prepared by combining various proportions of stock solutions of labeled and unlabeled ribose. Linear calibration curves were obtained for both deuterium and carbon-13 ribose samples.

KINETIC ISOTOPE EFFECTS:

Kinetic isotope effects for [1'-^{13}C], [2'-^{13}C], [1-^{15}N], [1'-^{2}H], [2'-^{2}H] and [5'-^{2}H] uridine are summarized in Table 1. The sites containing isotopes are shown in Figure 10. These

Figure 5: Synthesis of [5'-^{2}H] uridine.

a:DCC/DMSO; b:$NaBD_4$; c:1M HCl/heat (B=Uracil)

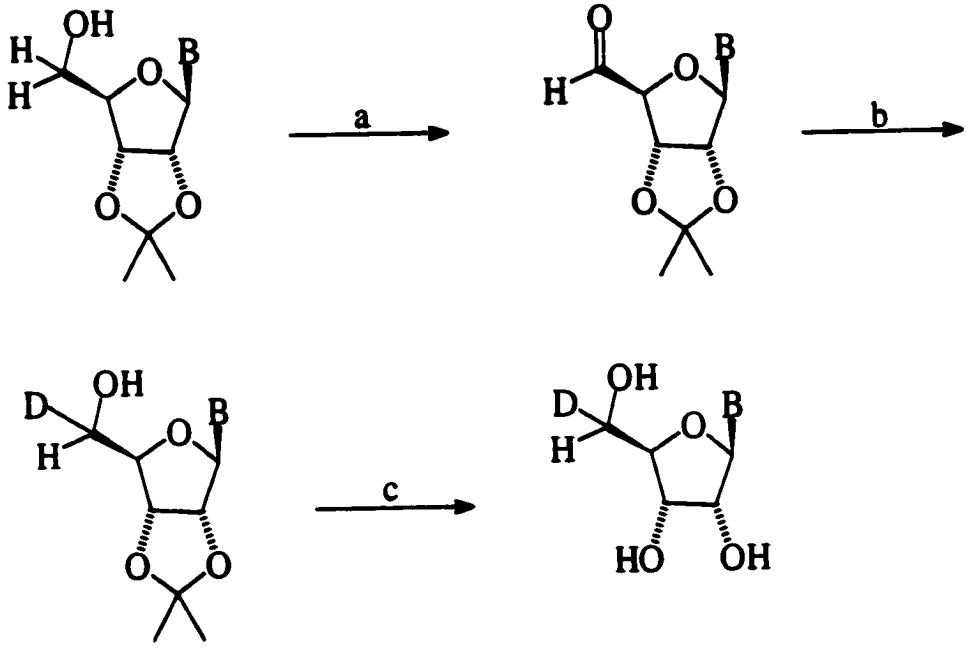

Figure 6: Synthesis of [1-^{15}N] uridine.

a:1)$KC^{15}N/K_2CO_3$, 2)HCl; b:H_2/HCl/PtO_2, 2)IR-45 (weakly basic) Resin; c:1)KCNO, 2)HCl; d:Br_2; e:heat; f:H_2/Pd/$BaSO_4$; g:$(Me_3Si)_2NH$; h:$CH_3CN/SnCl_4$

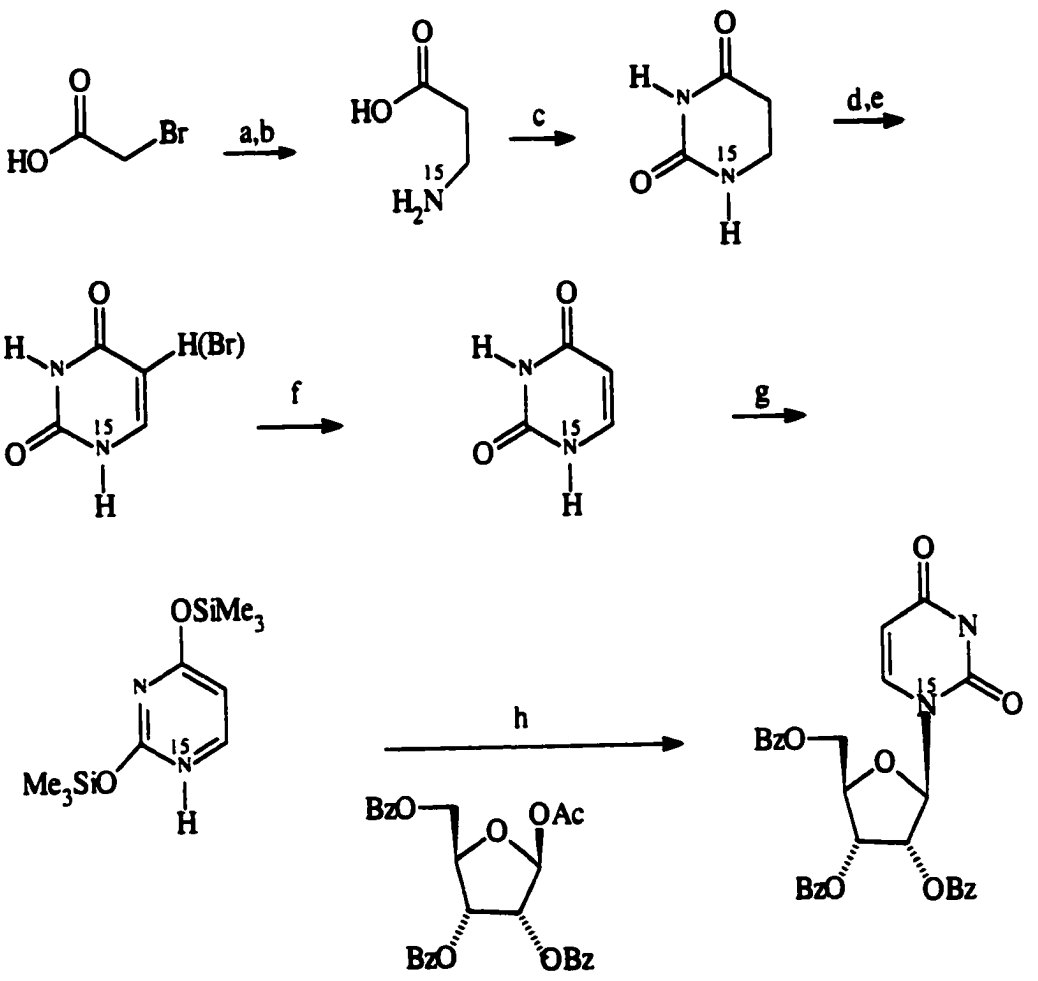

Figure 7: Mass spectrum of synthesized [1-^{15}N] uracil using method of Robert and Poulter.

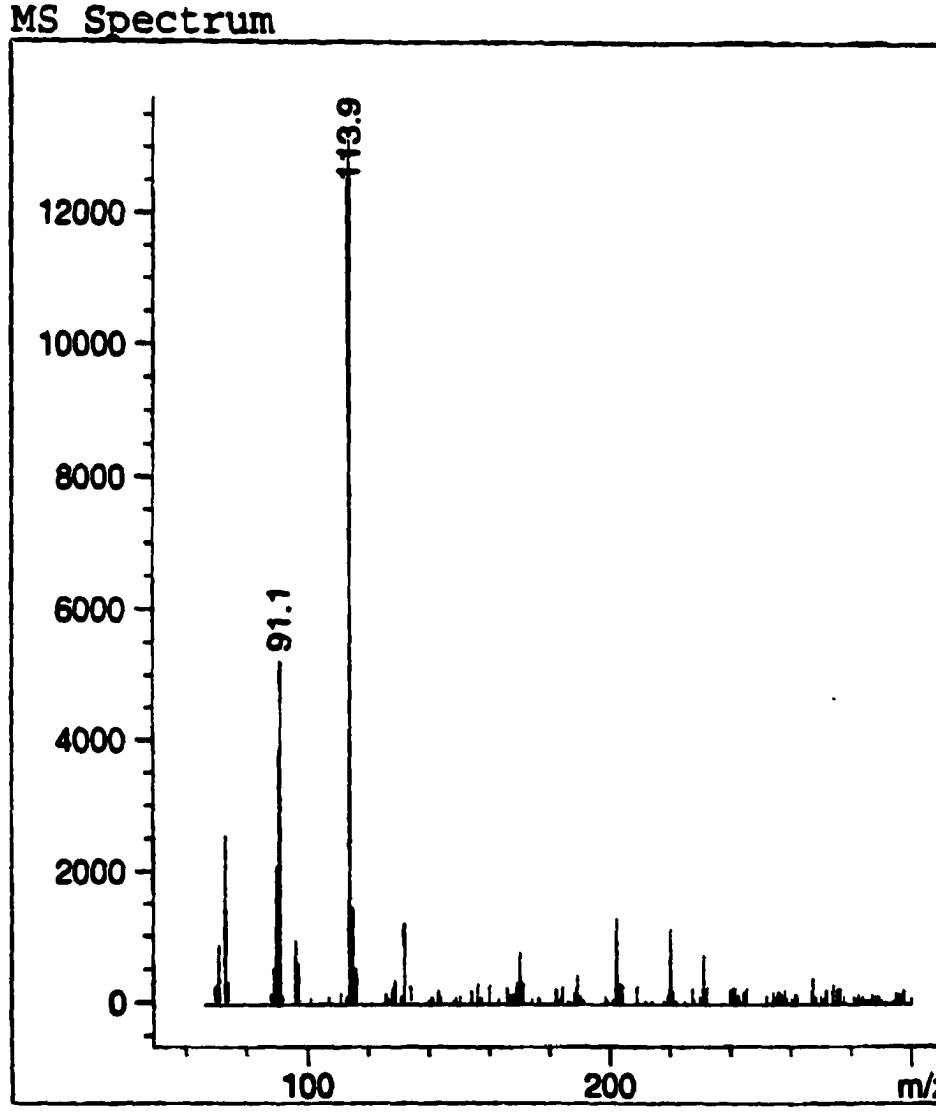

Figure 8: Calibration curve of [1-^{13}C] ribose: Relating observed isotopic enrichment to actual isotope content.

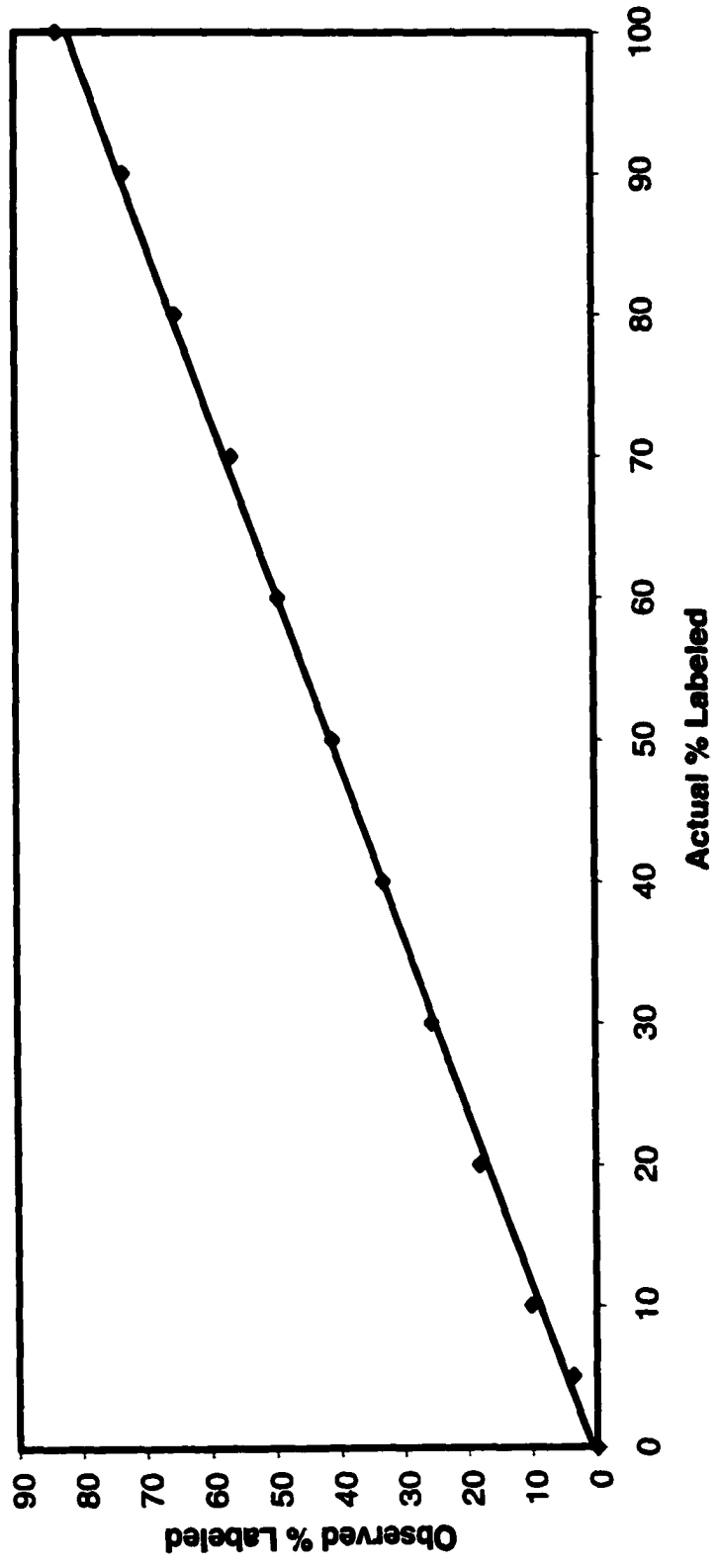

Figure 9: Calibration curve of [1-^{2}H] ribose: Relating observed isotopic enrichment to actual isotope content.

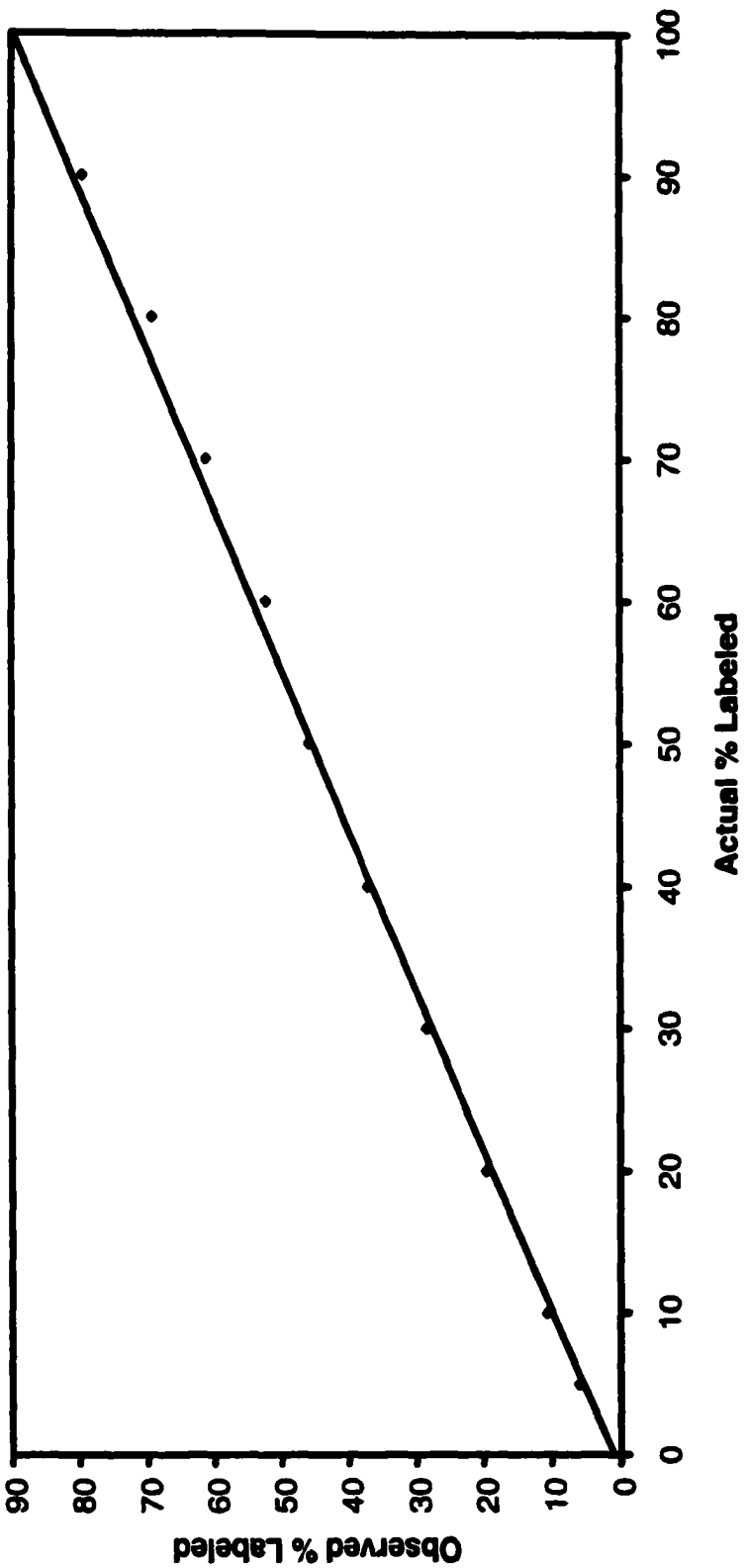

Figure 10: Structure of uridine with labeled sites.

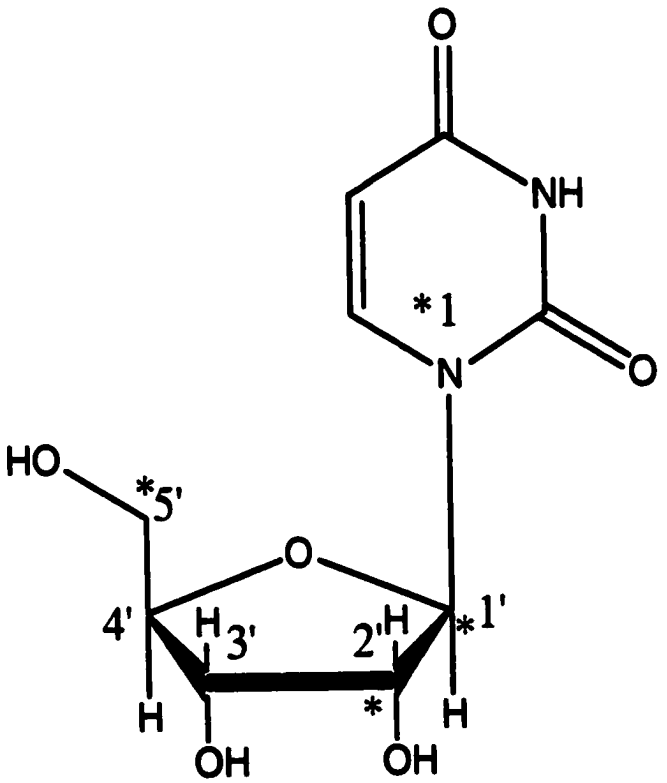

kinetic isotope effects are the average of a minimum of twenty analyses by LC/MS. Arsenolysis of uridine gave substantial secondary kinetic isotope effects for [1'-^{2}H], and significant [1'-^{13}C] and [1-^{15}N] primary effects. The isotope effects for the arsenolysis reaction are consistent with the dissociative character of the transition state in which C_1'-O_4' acquires oxocarbenium character and C_1' partially rehybridizes to sp^2. The substantial isotope effect for [1'-^{2}H] uridine might be due to protonation of O_2 that causes a decrease in the bond order of C_1'-H_1 The observed [1'-^{2}H] kinetic isotope effect of 1.144 $\pm$ 0.050 is equivalent to tritium KIE of 1.207 $\pm$ 0.050 using Swain-Schaad relationship. This KIE is higher than that observed for nucleoside phosphorylase (38). Formation of oxocarbenium ion character is another factor in observing a high [1'-^{2}H] isotope effect. The normal isotope effect at H_1' arises primarily from the increased freedom in the out-of-plane bending mode for H_1' at the transition state.

Protonation of O_2 in the uridine ring causes a change in the bond orders between N_1-C_1', C_1'-H_1', C_2'-H_2', and C_5'-H_5'. There is a decrease in the bond order between N_1-C_1' and C_1'-H_1' and an increase in the bond order between C_2'-$H_2'$and C_5'-H_5'. This increase in bond order accounts for the

Table 1. Kinetic isotope effects for thymidine phosphorylase.

Substrate	Type of effect	Experimental[1] kinetic isotope effect
[1'-^{13}C]	primary	1.013 ±0.007
[2'-^{13}C]	secondary	0.995 ±0.002
[1-^{15}N]	primary	1.027 ±0.046
[1'-^{2}H]	secondary	1.144 ±0.050
[2'-^{2}H]	secondary	0.959 ±0.012
[5'-^{2}H]	secondary	0.988 ±0.127

[1]These kinetic isotopes effects are the average of a minimum of twenty analyses by LC/MS.

inverse [2′-^{2}H] and [5′-^{2}H] kinetic isotope effect of 0.959 and 0.988 respectively. The dihedral angle of H_2′-C_2′-C_1′-N_1 changed from -27° at the ground state to 34° at the transition state reflecting a change from twist or half-chair C_2′-*exo*-C_3′-*endo* (N) to twist C_2′-*endo*-C_3′-*exo* (S) in the pseudorotational itinerary. The pseudorotation itinerary is another term for describing sugar puckering. The five-membered furanose ring is generally nonplanar. The ring can be puckered in an envelope (E) form with four atoms in a plane and the fifth atom is out of plane or in a twist (T) form with two adjacent atoms displaced on opposite sides of a plane through the other three atoms. Atoms displaced from these three-or four-atom planes and on the same side as C_5′ are called *endo;* those on the opposite side are called *exo*. This pseudorotation causes C_2′-H_2′ and C_1′-N_1 bonds to be slightly eclipsed at the transition state which also contributes to an inverse isotope effect at [2′-^{2}H] as well. This is in contrast to other nucleoside or nucleotide metabolizing enzymes such as AMP nucleosidase, nucleoside N-glycohydrolase, and nucleoside phosphorylase in which there is a near total eclipse resulting in the large [2′-^{2}H] isotope effect (37,38,39).

An isotope effect of 1.027 $\pm$ 0.046 for [1-^{15}N] is in close agreement with the reported value for nucleotide and nucleoside N-glycohydrolase and nucleoside hydrolase (39,38). However, breakage of the C_1'-N_1 bond is not as advanced as in the N-glycohydrolase reaction. This behavior has also been seen with nucleoside hydrolase (38).

TRANSITION STATE MODELING:

Following the determination of the kinetic isotope effects for the arsenolysis reaction using liquid chromatography/mass spectrometry, the values were matched to a transition state model selected by the BEBOVIB-IV program (47) developed by Sims and co-workers. This analysis is based on empirical relationships used in assigning force constants for angle bends and torsional coordinates, given certain structural information. Incorporating these relationships into the program allows the calculation of kinetic isotope effects for a preselected hypothetical transition state structure.

Six hypothetical transition state models based on the X-ray structure of *E. coli* thymidine phosphorylase and the proposed catalytic mechanism of thymidine phosphorylase were considered (13). All of the models were built using Spartan

and were energy minimized. The refinement of the models was carried out with Spartan 5 and Gaussian 98w. The Restricted Hartree-Fock (RHF) and Unrestricted Hartree-Fock (UHF) methods, with 3-21G* and 6-31G* basis set, were used for optimizing the models.

The following hypothetical transition states were modeled:

1. Protonation of O_2,
2. Hydrogen bonding to O_2,
3. Protonation of O_4,
4. Hydrogen bonding to O_4,
5. Protonation of O_2 and O_4, and
6. Protonation of O_2 and hydrogen bonding to O_4.

The following procedure was used to calculate the optimal geometry of the models:

1. Models were built using Spartan,
2. Geometry optimization was performed using Gaussian 98W, and
3. Cartesian coordinates obtained from the optimization were then transferred to BEBOVIB-IV and kinetic isotope effects calculated.

Results obtained from optimization of transition state models are as follows:

1. Protonation of O_2 resulted in a change of the conformation of the ribose ring from C_3'-*endo* to C_4'-*endo*-C_3'-*exo* on the furanose ring,
2. The initial C_3'-*endo* conformation of the furanose ring was maintained by hydrogen bonding to O_2,
3. Protonation of O_4 did not affect the conformation of the furanose ring,
4. Hydrogen bonding to O_4 did not affect the conformation of the furanose ring, and
5. Protonation of O_2 and O_4, and protonation of O_2 and hydrogen bonding to O_4 resulted in a change of the conformation of the ribose ring from C_3'-*endo* to C_4'-*endo*-C_3'-*exo*.

Based on the structural information from X-ray crystallography, the nucleoside could bind in a high energy conformation with an antiperiplanar glycosidic dihedral angle and C_4'-*endo* ribose pucker. Hydrogen bonding in the vicinity of almost 3 Å has been seen on O_2 and O_4 of the base ring as well. Unlike the crystallographic study, theoretical data indicate that O_2 has to be protonated rather than hydrogen bonded for the furanose ring to have a conformation of C_4'-*endo* and C_3'-*exo* (Figure 11). The

Figure 11: Structure of proposed transition state. This structure contains C_4'-*endo*-C_3'-*exo* conformation of furanose ring.

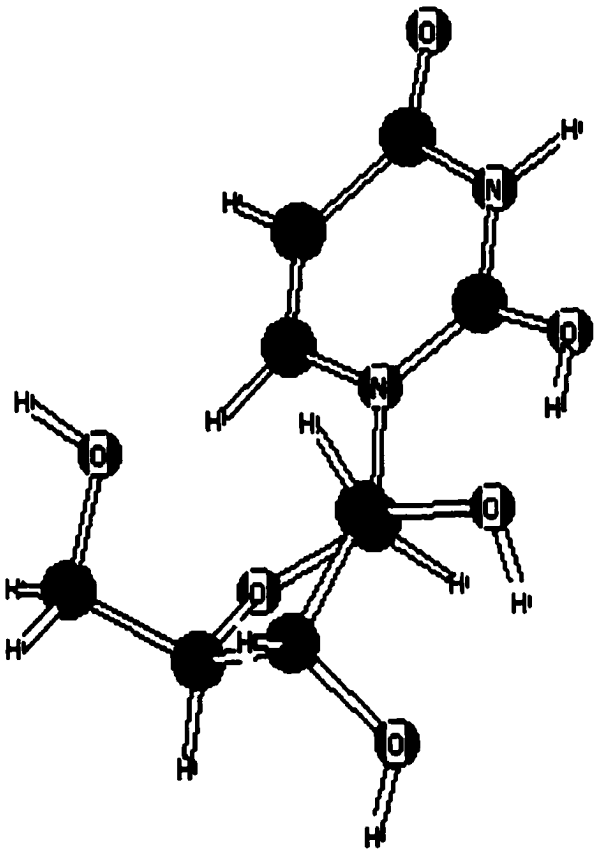

ground state structure for the truncated uridine used for the vibrational analysis of the transition state was in the C_3'-*endo* conformation as established by X-ray crystallography. This structure included ribosyl and imidazole ring moieties, but omitted all the hydroxyl hydrogen atoms on the furanose ring as well as 3', 4', and one of the 5' hydrogen atoms (Figure 12). However, the transition state configuration of the ribose ring changes from C_3'-*endo* to C_3'-*exo* as C_1' rehybridizes to an sp^2 carbon due to protonation of O_2 in the uracil ring.

Protonation of O_2 in the uracil ring also causes changes in bond orders and bond distances in both the uracil and furanose rings. There is a decrease in the bond order between N_1-C_1' and C_1'-H_1' from 1.059 to 0.78 and from 1.083 to 1.00, respectively. The bond order of C_2'-H_2' and C_5'-H_5' increased from 1.057 to 1.076, and from 1.048 to 1.051. This increased bond order resulted in inverse [2'-^{2}H] and [5'-^{2}H] kinetic isotope effects. There is a decrease of bond distances of N_1-C_2 and C_1'-O_4' from 1.376 Å to 1.324 Å, and from 1.393 to 1.357 Å, respectively. The decrease of bond distance of C_1'-O_4' is an indication of the formation of an oxocarbenium ion. Bond distances of N_1-C_6 and N_1-C_1'

Figure 12: Structure of uridine in the ground state. In this structure hydroxyl hydrogen atoms removed from the furanose ring as well as the 3', 4',and one of the 5' hydrogen atoms.

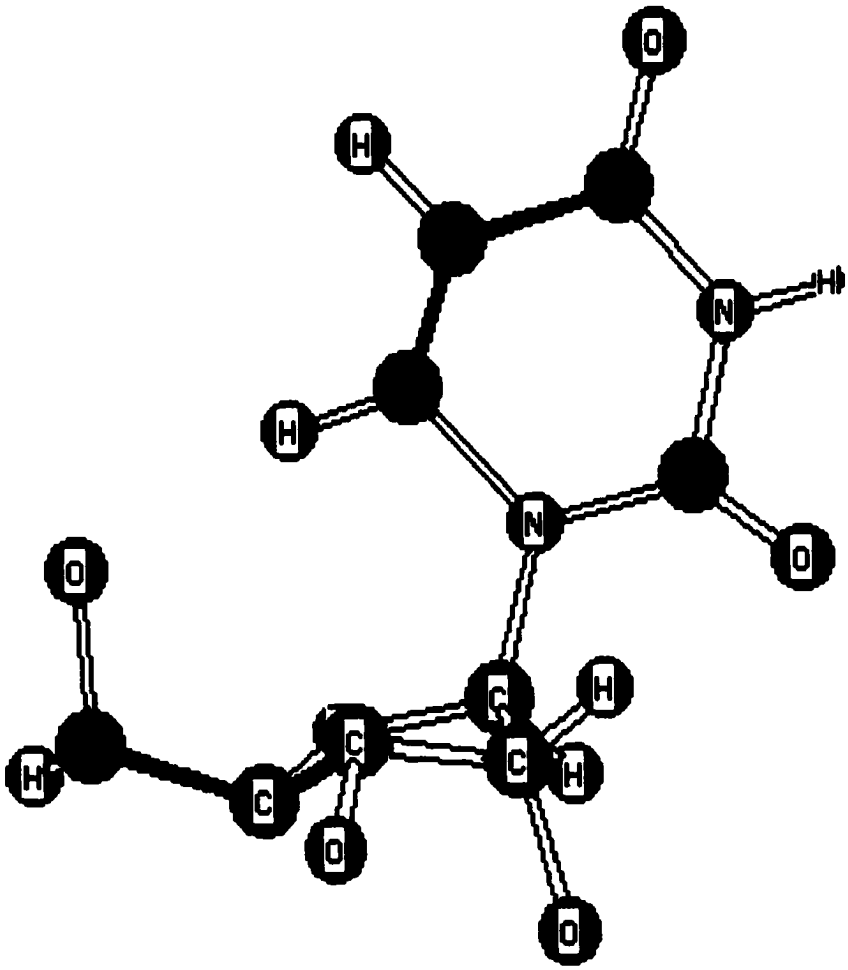

increased from 1.377 to 1.403 Å and from 1.474 to 1.568 Å, respectively.

Conformation of the ribose moiety is affected by protonation of O_2 in the uracil ring as well. Protonation of O_2 resulted in a change of the conformation of ribose from C_3'-*endo* to C_4'-*endo*-C_3'-*exo*. This C_4'-*endo* sugar pucker is similar to several purine nucleosides bound to purine nucleoside phosphorylase (PNP) (14).

Protonation of O_2 also changed the dihedral angle of O_4'-C_1'-N_1-C_1 from -162° at the ground state to -169° at the transition state. This change of dihedral angle leaves the pyrimidine nucleoside in an unusual high energy conformation that would likely put strain on the glycosidic bond. Glycosidic bond strain due to a high-energy nucleoside conformation is consistent with the catalytic mechanism proposed for the phosphorolysis of purine nucleosides (14). Protonation of O_2 also polarizes the N_1-C_1' glycosidic bond of the uridine to assist in the departure of uracil (Figure 13).

The cartesian coordinates obtained from all hypothetical transition state structures were imported into the BEBOVIB program to calculate KIEs. The experimental

Table 2. Comparison of experimental and theoretical kinetic isotope effects.

Substrate	Experimental KIE	PROTONATION		
		O_2	O_2 and O_4	O_2 and Hydrogen Bonding to O_4
[1'-^{13}C]	1.013±0.007	1.0309	1.0219	1.0242
[2'-^{13}C]	0.995±0.002	0.9998	1.0005	1.0004
[1'-^{15}N]	1.027±0.046	1.0033	1.0018	1.0094
[1'-^{2}H]	1.144±0.050	1.1564	1.1486	1.1357
[2'-^{2}H]	0.959±0.012	0.9260	0.9333	0.9283
[5'-^{2}H]	0.988±0.127	0.9943	0.9975	0.9961

KIEs are in close agreement with those calculated for the theoretical transition state with protonation at the O_2 position (Table 2). However, whether O_4 is protonated or hydrogen bonded is difficult to distinguish at this stage. Further research must be done. If the ribose moiety shows a C'_4-*endo* sugar pucker at the transition state based on the X-ray studies, this limits the conformations that can be present in the transition state to ones in which O_2 in the uracil ring is protonated.

Kinetic isotope effects are consistent with an S_N1-like transition state with oxocarbenium ion character, slight hyperconjugation between C_2'-H_2' and C_1'-N_1 bonds, and protonation of O_2 in the uracil ring. This leads to the following changes in both the uracil and furanose rings: C_4'-*endo*-C_3'-*exo* conformation in the ribofuranose ring; decrease of the dihedral angle of O_4'-C_1'-N_1-C_1; decrease of bond distances of N_1-C_2 and C_1'-O_4'; increase of bond distances of N_1-C_6 and N_1-C_1'; and polarization of N_1-C_1' glycosidic bond. From the BEBOVIB calculations, the ^{13}C isotope effect predicts a bond order of 0.78 for C_1'-N_1, indicating an early transition state.

ELECTROSTATIC POTENTIAL SURFACE OF TRANSITION STATES:

The molecular electrostatic potential has been shown to be a very useful tool for understanding the reactivity of molecules with ions or polar molecules, and the structure and energetics of intermolecular complexes including hydrogen bonded complexes. This computational method has provided an opportunity to investigate the electron density at the Van der Waals surface of substrates, and to compare it with that of the transition state structure. Hydrogen bonding and ionic interactions are two major electrostatic interactions that stabilize both enzyme-substrate and enzyme-transition state interactions. Electrostatic potential surfaces of enzyme-stabilized transition states could provide unique information for the design of transition state inhibitors. Electrostatic potential surfaces were calculated from the electron wave function for uridine, the proposed transition state, and a possible transition state analog. Figure 13 and 14 illustrates the electrostatic potential map of uridine and the proposed transition state respectively. Blue regions correspond to partial positive charge (electron deficient) and red regions correspond to partial negative charge (electron rich).

Figure 13: Electrostatic potential map of uridine. Blue regions correspond to partial positive charge and red regions correspond to partial negative charge.

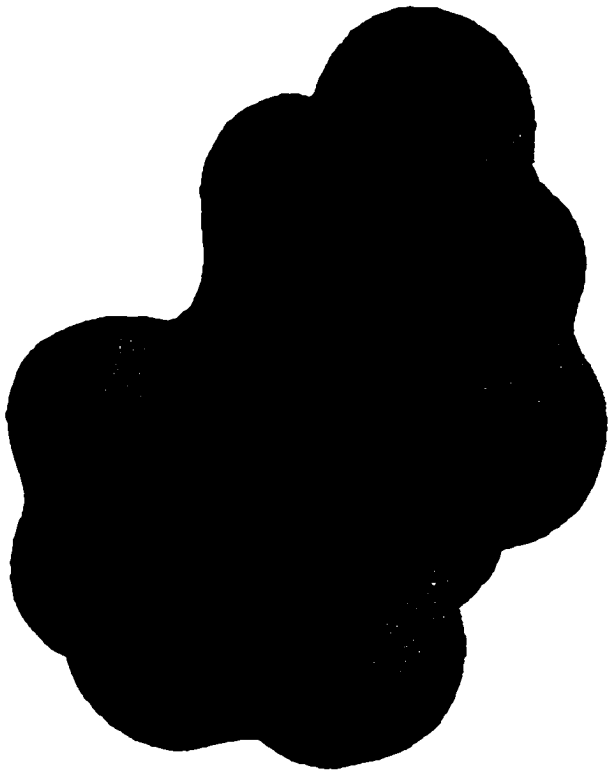

Figure 14: Electrostatic potential map of the proposed transition state. Blue regions correspond to partial positive charge and red regions correspond to partial negative charge.

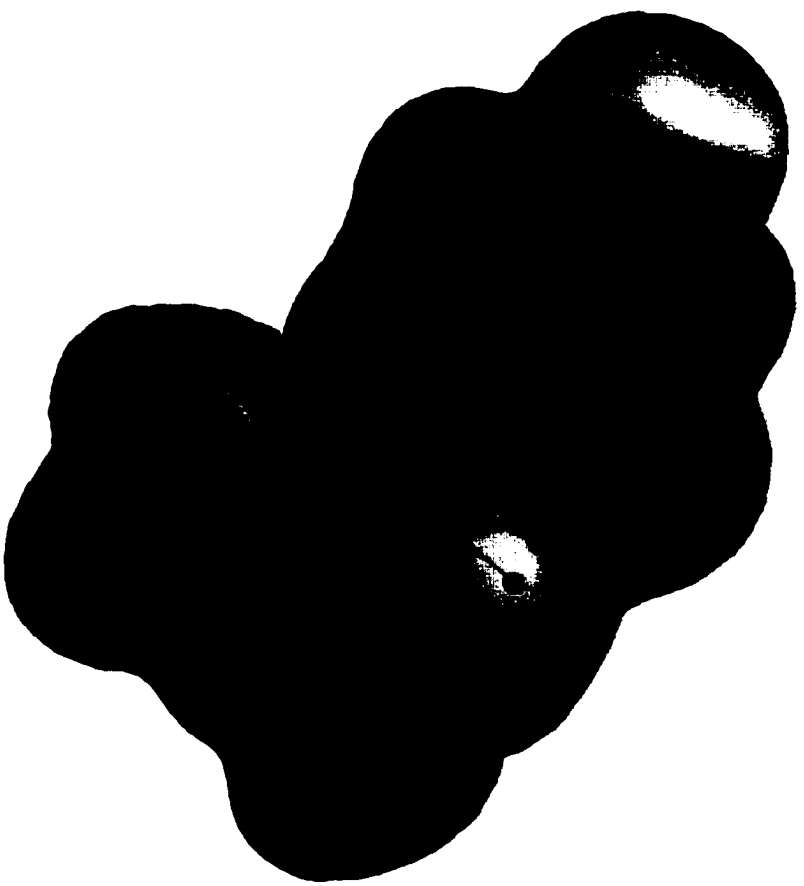

Note the formation of positive charge on N_1 in Figure 13.

INHIBITOR DESIGN BASED ON TRANSITION STATE ANALYSIS:

Many compounds having a structure similar to a substrate for a given enzyme will not be transformed by the enzyme, but will act as enzyme inhibitors. They are basically of two types, reversible and irreversible inhibitors. A reversible inhibitor can bind to the enzyme and subsequently be released, leaving the enzyme in its original condition. An irreversible inhibitor reacts with the enzyme to produce a protein that is not enzymatically active, and from which the original enzyme cannot be regenerated.

A unique class of reversible inhibitors is the transition state analog. They are stable products, designed to mimic the structure of an intermediate in the path of the substrate's transformation by the enzyme. They behave as very potent inhibitors, are not transformed into products, and have an association constant for the enzyme larger than the substrate itself. Since they are structurally mimicking the transition state of a chemical transformation, they are based on Pauling's postulate, whereby an enzyme recognizes

and binds more tightly to the transition state than to the ground state of the substrate product interconversion.

A possible transition state analog that can be considered is 4-[2'-deoxy-5',5'-(dimethyl)-β-D-ribofuranosyl]-[2,4]-quinazolinedione (Figure 15). The transition state analog's electrostatic potential surfaces were calculated from the electron wave function and compared with the proposed transition state (Figure 16). The results demonstrate a convincing match of geometry and electrostatic charges. Note the charge distribution (electron rich and electron deficient) on both the uracil and ribofuranose rings and ribofuranose conformation (C_4'-*endo*-C_3'-*exo*).

Figure 15: Structure of 4-[2'-deoxy-5',5'-(dimehtyl)-β-D-ribofuranosyl]-[2,4,]-quinazolinedione. A possible transition state analog for thymidine phosphorylase.

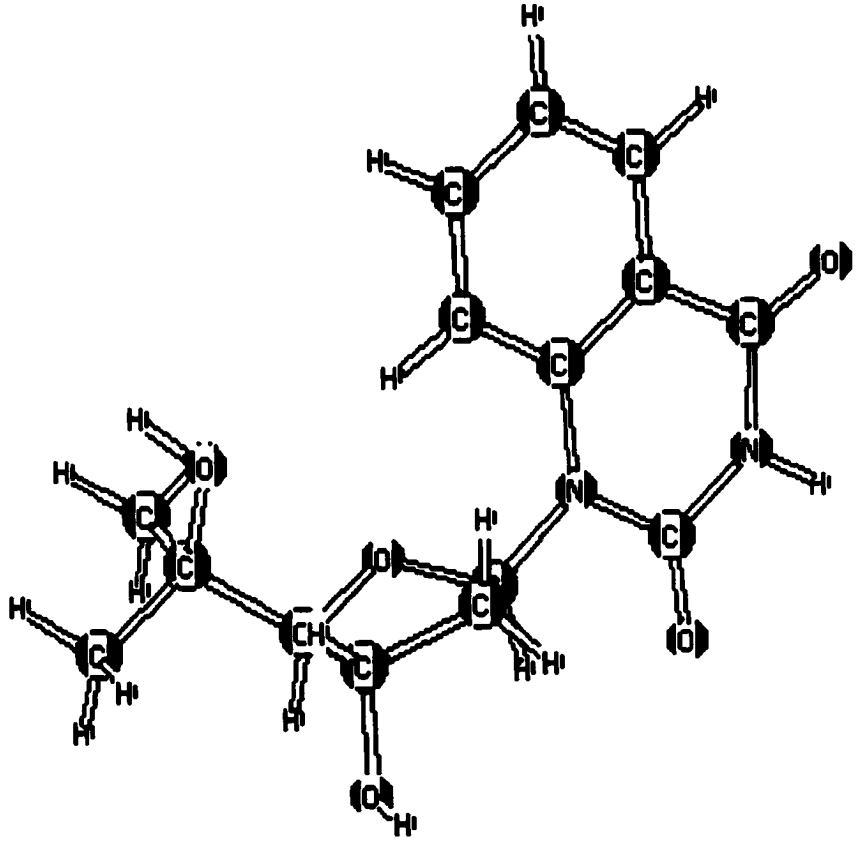

Figure 16: The electrostatic potential map of the 4-[2'-deoxy-5',5'-(dimethyl)-β-D-ribofuranosyl]-[2,4]-quinazolinedione. Blue regions correspond to partial positive charge and red regions correspond to partial negative charge.

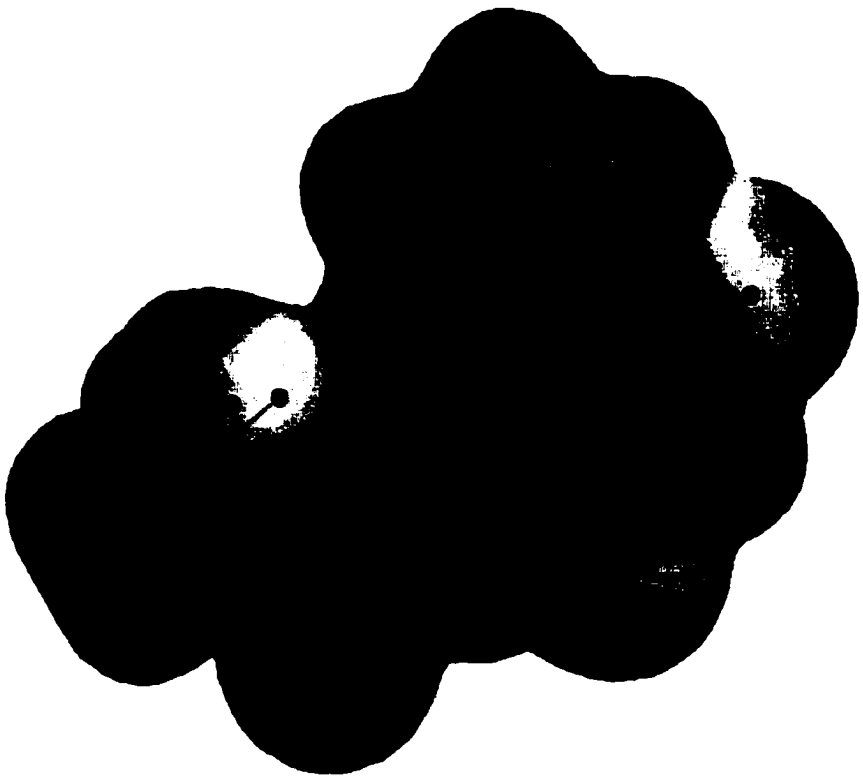

CHAPTER FOUR

CONCLUSION

Sequential applications of experimental and computational methods were used to analyze the transition state of thymidine phosphorylase. The experimentally determined kinetic isotope effects obtained for [1'-^{2}H], [2'-^{2}H], [5'-^{2}H], [1'-^{13}C], [2'-^{13}C], and [1-^{15}N] uridine are 1.144 $\pm$ 0.050, 0.959 $\pm$ 0.012, 0.988 $\pm$ 0.127, 1.013 $\pm$ 0.007, 0.995 $\pm$ 0.002, and 1.027 $\pm$ 0.046 respectively. These experimental kinetic isotope effects obtained for the arsenolysis reaction were matched to a vibrational transition state using energy-bond order vibrational analysis.

An acceptable transition state was one in which the experimentally observed isotope effects were matched to the kinetic isotope effects calculated for a specific model of transition-state vibrational structure and geometry. The procedure to select the appropriate transition state was based on the structural information from the study of *E. coli* TP with X-ray crystallography and proposed catalytic mechanism of thymidine phosphorylase. The range of acceptable transition states is defined in part by the requirement for a C_4'-*endo* sugar pucker. This limits the

conformations that can be present in the transition state to ones in which the O_2 in the uracil ring has to be protonated. Protonation of O_2 in the uracil ring causes a change in the conformation of the furanose ring and also assists departure of the uracil.

Kinetic isotope effects are consistent with an S_N1-like transition state with oxo-carbenium ion character; slight hyperconjugation exists between the C_2'-H_2' and C_1'-N_1 bonds; C_4'-*endo* and C_3'-*exo* conformation of furanose ring due to protonation of O_2 in the uracil ring; and the bond order of 0.78 for C_1'-N_1 indicating an early transition state.

Transition state analog was designed based on the information from experimental and theoretical calculations.

CHAPTER FIVE

EDUCATIONAL IMPLICATIONS

The discipline of biochemistry is highly complex and often quite abstract. Transition state analysis and molecular modeling is a prime example of the kind of material which presents a formidable task to the chemical educator.

Efforts to teach chemistry at the high school and undergraduate levels can be enhanced by reflecting on the current understanding of the variety of ways that students learn. The Theory of Multiple Intelligences (MI) can assist the educator in designing a course which maximizes the variety of learning opportunities, in order to reach the greater proportion of students.

The Theory of Multiple Intelligences (MI) provides an opportunity to transcend mere variation and selection. The MI approach can be useful in determining which analogies, which examples, and what activities are most likely to communicate the essential aspects of the topics. Gardner affirms the importance of the "hands-on" approach to education (60,61).

In the arts and crafts, students learn by doing. To learn about painting, students paint; to learn to operate a table saw, they operate a table saw.

In the sciences students learn almost entirely by reading and performing laboratory experiments. Although these students review the procedures and findings of pivotal experiments, they do not design and conduct their own experiments. The Theory of Multiple Intelligences suggests that there are a number of shortcomings when education is restricted as it traditionally is in the sciences. The heavily verbal context favors students who excel in the linguistic intelligence while at the same time it hinders the use of other intelligences (61).

Multiple Intelligence theory can be implemented in the undergraduate biochemistry classroom through the use of molecular modeling. Molecular modeling is a major new learning and teaching tool, and is already well established as an essential chemical research tool. Teachers can integrate molecular modeling in virtually every aspect of elementary chemistry, and students can actually use powerful molecular modeling techniques to help them grasp

difficult concepts that cannot be obtained merely by reading (62).

LITERATURE REVIEW:

Every society constructs its ideal human being. The ancient Greeks valued the person who displayed physical agility, rational judgment, and virtuous behavior. The Romans highlighted courage, and followers of Islam praised the holy soldier. Under the influence of Confucius, Chinese populations traditionally valued the person who was skilled in poetry, music, calligraphy, archery, and drawing. Among the Keres tribe of the Pueblo Indians today, the person who cares for others is held in high regard (61).

Western academics admire, promote, and sometimes attempt to measure "intelligence." Intelligence can be defined as the ability to solve problems, utilize logic, and think critically, as the ability to respond successfully to new situations and the capacity to learn from past experiences.

If one's car breaks down on the highway, who is the most intelligent person for the job? Is it someone with a

Ph.D. from a great university or a car mechanic with a junior high school education? If one gets lost in a large city, who's likely to be of greater help, an absent-minded professor or a little boy with a great sense of direction? Intelligence depends on the context, the tasks, and the demands that life presents, and not on an IQ score, a college degree, or a prestigious reputation (61).

The traditional understanding of intelligence assumes that our ability to learn and to perform tasks arises from a uniform cognitive capacity. Some researchers began to believe that such an intelligence would be fairly easy to measure and thus, be useful in assessing students in order to place them at an appropriate academic level. At the turn of the 20th century, educators in Paris asked psychologist Alfred Binet to formulate a test which could be used to analyze a child's intelligence in order to uncover his or her weaknesses. The Intelligence Quotient, or IQ test, was thus born.

Advocates of traditional education continue to push this paradigm of uniform schooling: an educational system based on national standards and efficient, cost-effective assessments in the form of pencil and paper tests using

objective questions. Against this long-lived convention, though, many researchers, educators, even parents, have expressed the reservation that such tests do nothing to judge a student's actual potential. Many believe these tests merely demonstrate that a child is or is not good at taking standardized tests. These standardized tests often fail to indicate how students will do after they get out into the "real world". One study of highly successful professional people indicated that fully one third of these professionals had low IQ scores. The message is clear: IQ tests have been measuring something that might be more properly called "schoolhouse giftedness", while real intelligence may take in a much broader range of skills (60,61).

Intelligence is not a magical cerebral substance that could be measured by an IQ test, nor is it a golden chromosome given at birth to a few lucky individuals. Intelligence could instead be more clearly defined as the multiple intelligences that can be utilized in every walk of life. Howard Gardner defined intelligence as a single general capacity possessed by every individual to a greater or lesser extent. Amassing a wealth of evidence, Gardner

posits the existence of a number of intelligences that ultimately yield a unique cognitive profile for each person (64).

Multiple Intelligence theory is a pluralized way of understanding the intellect. Recent advances in cognitive science, developmental psychology, and neuroscience suggest that each person's level of intelligence, as it has been traditionally considered, is actually made up of autonomous faculties that can work individually or in concert with other faculties. Howard Gardner originally identified seven such faculties; he later added an eighth intelligence: (1) linguistic; (2) logical-mathematical; (3) spatial; (4) musical; (5) bodily-kinesthetic; (6) interpersonal; (7) intrapersonal; (8) naturalist (63,64).

Gardner's first form of intelligence, linguistic intelligence, is the intelligence of words. This is the intelligence of the journalist, storyteller, poet, and lawyer. Linguistic intelligence is the form of thinking that brought us Shakespeare's *King Lear*, Homer's *Odyssey*, and the *Tales of the Arabian Nights*. People who are particularly gifted in this area can argue, persuade, entertain, or instruct effectively through the spoken word.

Those with verbal intelligence often love to play with the sounds of language through puns, word games, and tongue twisters. People with this intelligence may be trivia experts because of their ability to retain facts, or they may be highly literate. They may read voraciously, write clearly, and gain meaning in other ways through print.

Gardner's second intelligence is logical-mathematical. This ability is the intelligence of numbers and logic. This is often the intelligence of the scientist, accountant, and computer programmer. Newton tapped into logic and mathematics when he invented calculus. Einstein used this intelligence when he developed his theory of relativity. Traits of a logical-mathematically inclined individual include the ability to reason, to sequence, to think in terms of cause-and-effect, to create hypotheses, to look for conceptual regularities of numerical patterns, and to enjoy a generally rational outlook on life.

Third, is spatial intelligence. Spatial intelligence involves thinking in pictures and images and the ability to perceive, transform, and re-create different aspects of the visual-spatial world. Spatial intelligence is the playground of architects, photographers, artist, pilots,

and mechanical engineers. Those who designed the pyramids in Egypt must have had spatial intelligence. Other individuals who have displayed this intelligence are Thomas Edison, Pablo Picasso, and Ansel Adams. Highly spatial individuals often have an acute sensitivity to visual details and can visualize vividly, draw or sketch their ideas graphically, and orient themselves in three-dimensional space with ease.

Musical intelligence is the fourth type of intelligence. Key features of musical intelligence are the capacity to perceive, to appreciate, and to produce rhythms and melodies. This may be the intelligence of a Bach, Beethoven, or Brahms. A Balinese gamelan player or a Yugoslavian epic singer may also display musical intelligence. Musical intelligence also resides in the mind of any individual who can sing in tune, keep time to music, and listen to different musical selections with some degree of discernment.

The fifth intelligence, bodily-kinesthetic, is the intelligence of the physical self. A person with this intelligence may be adept at controlling body movements and in handling objects skillfully. Athletes, craftspeople,

mechanics, and surgeons may possess a great measure of bodily kinesthetic intelligence. Charlie Chaplin may have drawn upon it in order to perform his many ingenious routines. Bodily-smart individuals may be skilled in sewing, carpentry, or model-building. They may enjoy physical pursuits like hiking, dancing, jogging, camping, swimming, or boating. These people tend to have good tactile sensitivity, need to move their bodies frequently, and have intuitive or "gut reactions" to situations.

Gardner's sixth intelligence is interpersonal. This is the ability to understand and work with other people. In particular, interpersonal intelligence requires a capacity to perceive and be responsive to the moods, temperaments, intentions, and desires of others. A social director on a cruise ship would benefit from this intelligence, as would an administrator of a large corporation. An interpersonally intelligent individual may be very compassionate and socially responsible, like Mahatma Gandhi, or manipulative and cunning like Machiavelli. One with interpersonal intelligence may have the ability to get "inside the mind" of another person and

view the world from that individual's perspective. As such, they make wonderful negotiators and teachers.

The seventh intelligence is intrapersonal, or the intelligence of the inner self. A person strong in this type of intelligence can easily access his own feelings, discriminate between different kinds of inner emotional states, and use his self-understanding to enrich and guide his life. Examples of individuals intelligent in this way include counselors, theologians, and self-employed business people. Intrapersonal intelligent people may be very introspective and enjoy meditation and contemplation. They might be fiercely independent, highly goal-directed, and intensely self-disciplined. Intrapersonally intelligent people prefer to work on their own rather than with others.

Recently, Gardner added an eighth category, the naturalist intelligence. The naturalist intelligence is the ability that allows recognition and classification of things in the natural world (and perhaps the artificial world). This is the intelligence of the biologist, farmer, forester, and ranger (65).

In addition to these types of intelligences, researchers of MI believe that the process of learning is

both wondrous and complex. They are attempting to explain how the brain works and to redefine learning itself. They have found that brain activity occurs in a number of ways: spontaneously, automatically, and in response to challenge. To learn effectively, this brain activity must be stimulated in at least one of these ways and then combined with useful and suitable feedback systems. Moreover, for learning to continue, the brain must be provided challenging tasks that require significant amounts of reflection or emotional energy. This challenge is an important part of healthy brain functioning (60).

Applying MI in the chemistry classroom:

What would it be like to teach a college-level class in which students are assisted in identifying, acknowledging and stimulating different ways of being "intelligent?". MI theory contends that many of the brightest and most capable learners are caught in a system that places heavy emphasis on linguistics (word-smart intelligence) and logical-mathematical, (number-and-computer-smart intelligence). Higher education traditionally emphasizes these two approaches. Focusing

solely on these types of learning strategies has encouraged rote-memory teaching that fosters low motivation and poor performance. Many students thought to be lazy are actually bored and frustrated. Though they are "smart," they are craving multiple methods of stimulation-methods that may be more effective in helping them master course material (64).

Molecular modeling can be integrated into the undergraduate biochemistry classroom to explore some of these MI assumptions. The traditional approach to teaching biochemistry, particularly in the dynamic aspect of biochemical reactions (such as the behavior of proteins and enzymes), is limited to lecture. Molecular modeling, which can be considered as a procedure of social learning, can be employed in the biochemistry classroom and laboratory as well as presented as specific examples of actual lecture "demonstrations" and laboratory "experiments". This type of social learning may serve both as a template and as a catalyst for continued development of materials for the undergraduate biochemistry curriculum.

Lecture demonstrations can be prepared using Wavefunction's Spartan molecular modeling program (66), which provides access to a wide variety of molecular

mechanics and quantum chemical techniques as well as an impressive array of graphic displays. The laboratory exercises can be designed to be carried out using Spartan, or using MacSpartan or PC Spartan for Power MacIntosh and Windows 95/NT based personal computers.

Molecular modeling may be employed either as a means to learn and understand chemistry, or as a tool to explore chemistry (66). The two are often one and the same. Use of molecular modeling in the undergraduate chemistry curriculum to examine and explore relationships between molecular structure and molecular properties is particularly exciting. This fundamental theme of structure and property relationships pervades almost every stage of a chemist's education.

Molecular modeling is much more than a pretty picture. Three-dimensional molecular structures, displayed and manipulated in real time, offer significant advantages over static two-dimensional line drawings. Electron distributions may also be portrayed, allowing quantitative descriptions of molecular size and shape, as well as elucidation of chemical bonding. Electrostatic potentials directly convey information about molecular charge

distribution, and reveal likely sites for electrophilic and nucleophilic reactivity. In short, molecular modeling opens up a treasure of information for both chemists and students of chemistry (66).

Molecular modeling helps students to understand the phenomenon of a biochemical reaction. This approach allows description of the bonding in the transition state, about which no direct information can be obtained from experiments. Molecular modeling is not limited to static pictures. "Movies" can be used to depict vibrations in stable molecules, as well as the motions which molecules undergo during reaction (66).

Students learn by hands-on experiences, which may include performing some exercise such as drawing a molecular structure, performing energy minimization, and measuring bond angles and dihedral angles on a structure. This illustrates students processing knowledge through bodily sensations (the fifth intelligence). They respond best in learning situations that provide manipulative action exercises, and hands-on learning experiences. Molecular modeling also improves students' spatial intelligence. Students' spatial abilities can be improved

by having them visualize objects in a rotated configuration.

CONCLUSION:

Learning is a fascinating interactive process--the product of student and teacher activity within a specific learning environment. These activities, which are central elements of the learning process, show wide variation in pattern, style, and quality. In reality, however, the academic paradigm in many schools has not changed much over the years. The public, the press, and even many in the profession have a generally simplistic view of the relationship between the process of teaching, and the outcomes of student achievement.

Many educators also think of instruction and learning as directly related. If the one is present to an acceptable degree, the other should naturally follow. If the teacher is working hard, students should learn. If they do not, an earlier generation blamed the student while the current trend is to hold the teachers, administrators, and school system accountable. The reality is considerably more complex.

Professors, teachers or mentors should use several methods to achieve instructional effectiveness. Their teaching should involve a variety of communication techniques. Principally, learning occurs from hearing (linguistic intelligence): lecture, discussion, conversation, dramatization; seeing (spatial intelligence and interpersonal): reading, displays, visual aids, demonstration; and doing (bodily-kinesthetic): trial and error, experimenting, and copying the acts of others. As each task, skill, or idea is broken down into simple steps, the learner can confirm what she or he knows, needs to know, and wants to know. Thus, learning is actually a series of discoveries. Each step should lead to some success. The learner must be encouraged, so that progress is made (66).

Teaching science in general, and chemistry in particular, is difficult in an era of decreasing attention. No longer is the traditional teaching method sufficient. Teachers may use traditional teaching methods because that is how they were taught. Effective teaching is complicated, difficult, and time consuming. In order to maintain the energy and commitment for teaching

effectively, teachers have to employ different methods in their classes. Multiple Intelligence theory can be implemented in the chemistry classroom through the use of molecular modeling. Students will learn the basic information about enzymes and their reactivity from lecture (linguistic intelligence) and incorporate that information in the laboratory by using molecular modeling (spatial intelligence and bodily-kinesthetic). Students may also need to work in pairs to utilize their interpersonal skills by verbalizing their ideas, as well as considering input from others.

APPENDIX

Input file sample:

```
Mansoureh Rezaei Thymidine Phophorylase expanded sn2 with inversion.
Aug 21, 1998.  This file incorporates the geometry at C5' of uridine
into the TS model.
   23   68    0    7    1    1    303.0
    1    15.0
    1    1   13   18    0    0    1    2
    2    1   23   18    0    0    1    2
    3    1   18   17    0    0    1    2
    4    1   17   22    0    0    1    2
    5    1   13   14    0    0    1    2
    6    1   19   14    0    0    1    2
    7    1   14   15    0    0    1    2
    8    1   15   20    0    0    1    2
    9    1   15   16    0    0    1    2
   10    1   16   21    0    0    1    2
   11    1   16   17    0    0    1    2
   12    1    1   13    0    0    1    2
   13    1    1    6    0    0    1    2
   14    1    1    2    0    0    1    2
   15    1    1    7    0    0    1    2
   16    1    2    8    0    0    1    2
   17    1    2    9    0    0    1    2
   18    1    2    3    0    0    1    2
   19    1    3   10    0    0    1    2
   20    1    6    4    0    0    1    2
   21    1    3    4    0    0    1    2
   22    1    4    5    0    0    1    2
   23    1    5   11    0    0    1    2
   24    1    5   12    0    0    1    2
   25    2   13   18   23    0    1    3
   26    2   13   18   17    0    1    3
   27    2   13   14   19    0    0    3
   28    2   13   14   15    0    1    3
   29    2   23   18   17    0    1    3
   30    2   18   17   16    0    1    3
   31    2   17   16   15    0    1    3
   32    2   18   13   14    0    1    3
   33    2   19   14   15    0    1    3
   34    2   21   16   15    0    1    3
   35    2   21   16   17    0    1    3
   36    2   20   15   14    0    1    3
   37    2   20   15   16    0    1    3
   38    2   22   17   16    0    1    3
   39    2   22   17   18    0    1    3
   40    2    1    7   13    0    1    3
   41    2    7    1    6    0    1    3
   42    2    7    1    2    0    1    3
   43    2    1    6    4    0    1    3
   44    2    1    2    3    0    1    3
   45    2    1    2    8    0    1    3
   46    2    1    2    9    0    1    3
```

```
   47    2    9    2    8    0    1    3
   48    2    1   13   18    0    1    3
   49    2    1   13   14    0    1    3
   50    2    8    2    3    0    1    3
   51    2    9    2    3    0    1    3
   52    2    2    1    6    0    1    3
   53    2    6    1   13    0    1    3
   54    2    2    1   13    0    1    3
   55    2    2    3    4    0    1    3
   56    2    5    4    6    0    1    3
   57    2    5    4    3    0    1    3
   58    2   11    5   12    0    1    3
   59    2   12    5    4    0    1    3
   60    5    8    2    1   13    0    4
   61    5    6    1   13   14    0    4
   62    5    7    1   13   18    0    4
   63    5    2    1    6    4    0    4
   64    5   19   14   13    1    0    4
   65    5    3    2    1    6    0    4
   66    5    3    2    1    7    0    4
   67    5    6    4    5   11    0    4
   68    5    2    1   13   18    0    4
   5.200     5.000     4.500     5.000     5.200     5.300     5.200
4.500
   5.200     5.300     4.500     5.200     5.300     4.500     5.000
5.000
   5.300     4.500     5.300     5.300     4.500     4.500     5.300
5.000
   0.650     0.650     1.250     0.650     0.650     1.000     0.650
1.250
   1.250     1.250     1.250     0.650     0.650     0.650     0.650
0.650
   0.650     0.650     0.650     1.250     0.650     1.250     0.650
1.250
   1.250     0.650     1.250     1.250     1.250     1.000     1.250
1.000
   1.250     0.750     0.650     0.024     0.024     0.024     0.024
0.024
   0.024     0.024     0.024     0.024
   23    1    2
    12.0      12.0      12.0      12.0      12.0      16.0      1.0
1.0
    16.0      16.0      16.0      1.0       14.0      12.0      14.0
12.0
    12.0      12.0      16.0      1.0       16.0      1.0       1.0
    13.0      12.0      12.0      12.0      12.0      16.0      1.0
1.0
    16.0      16.0      16.0      1.0       14.0      12.0      14.0
12.0
    12.0      12.0      16.0      1.0       16.0      1.0       1.0
    12.0      13.0      12.0      12.0      12.0      16.0      1.0
1.0
```

```
    16.0       16.0       16.0       1.0        14.0       12.0       14.0
12.0
    12.0       12.0       16.0       1.0        16.0       1.0        1.0
    12.0       12.0       12.0       12.0       12.0       16.0       1.0
1.0
    16.0       16.0       16.0       1.0        15.0       12.0       14.0
12.0
    12.0       12.0       16.0       1.0        16.0       1.0        1.0
    12.0       12.0       12.0       12.0       12.0       16.0       2.0
1.0
    16.0       16.0       16.0       1.0        14.0       12.0       14.0
12.0
    12.0       12.0       16.0       1.0        16.0       1.0        1.0
    12.0       12.0       12.0       12.0       12.0       16.0       1.0
2.0
    16.0       16.0       16.0       2.0        14.0       12.0       14.0
12.0
    12.0       12.0       16.0       1.0        16.0       1.0        1.0
    12.0       12.0       12.0       12.0       12.0       16.0       1.0
1.0
    16.0       16.0       16.0       2.0        14.0       12.0       14.0
12.0
    12.0       12.0       16.0       1.0        16.0       1.0        1.0
Normal Isotopes
Primary C-13
Secondary C-13
primary N-15
Secondary H-2 1'
Secondary H-2 2'
Remote H-2 5'
uridine STRUCTURE FROM CRYSTAL DATA: Acta Cryst B26, p 1101, 1970
Model.  SUM C1' BO = 4.107  Hydrogen BO's from ampa

     1     0     3 C-1  0.000       0.0        0.0       1.000
    13     0     3 N-13 1.492      73.549     21.192     1.059
     6     0     3 O-6  1.445     110.716   -233.637     1.188
     2     0     3 C-2  1.509      41.140   -142.320     0.928
     7     0     3 H-7  1.100     135.440    -76.668     1.083
     4     6     3 C-4  1.445      58.988   -187.481     1.371
     5     4     3 C-5  1.509      88.549   -254.767     0.993
     3     4     3 C-3  1.506      27.958    -65.780     0.951
    10     3     3 O-10 1.445      64.141   -161.233     1.152
     9     2     3 O-9  1.445     112.847   -127.907     1.182
    11     5     3 O-11 1.445      58.921     37.301     1.146
    14    13     3 C-14 1.492      83.659    -42.688     1.553
    18    13     3 C-18 1.492      83.201     79.599     0.612
    19    14     3 O-19 1.445      96.653    -98.906     2.278
    15    14     3 N-15 1.492      75.979     22.925     1.515
    16    15     3 C-16 1.492      81.931     75.713     1.486
    20    15     3 H-20 1.008      83.570    -42.569     1.403
    17    16     3 C-17 1.509      97.405   -218.911     1.197
    21    16     3 O-21 1.445      75.841     15.911     2.299
    22    17     3 H-22 1.100      83.313     80.960     1.103
```

```
 23   18    3 H-23 1.100      97.144  -211.692    0.679
  8    2    3 H-8  1.100      43.646   -30.625    1.057
 12    5    3 H-12 1.100     159.735  -258.147    1.048
  2    3    0 C-2  1.509                          0.936
 13   18    0 N-13 1.492                          1.465
```

Transition State ts couples reaction coordinate with walden inversion 30 degrees. Protonation of O_2, C_5' hydroxymethyl geometry of ino part of TS model.

```
 24   70   0    7     3    1    303.0
  1    15.0
  1    1   13   18    0    0    1    2
  2    1   23   18    0    0    1    2
  3    1   18   17    0    0    1    2
  4    1   17   22    0    0    1    2
  5    1   13   14    0    0    1    2
  6    1   19   14    0    0    1    2
  7    1   14   15    0    0    1    2
  8    1   15   20    0    0    1    2
  9    1   15   16    0    0    1    2
 10    1   16   21    0    0    1    2
 11    1   16   17    0    0    1    2
 12    1    1   13    0    0    1    2
 13    1    1    6    0    0    1    2
 14    1    1    2    0    0    1    2
 15    1    1    7    0    0    1    2
 16    1    2    8    0    0    1    2
 17    1    2    9    0    0    1    2
 18    1    2    3    0    0    1    2
 19    1    3   10    0    0    1    2
 20    1    6    4    0    0    1    2
 21    1    3    4    0    0    1    2
 22    1    4    5    0    0    1    2
 23    1    5   11    0    0    1    2
 24    1    5   12    0    0    1    2
 25    2   13   18   23    0    1    3
 26    2   13   18   17    0    1    3
 27    2   13   14   19    0    0    3
 28    2   13   14   15    0    1    3
 29    2   23   18   17    0    1    3
 30    2   18   17   16    0    1    3
 31    2   17   16   15    0    1    3
 32    2   18   13   14    0    1    3
 33    2   19   14   15    0    1    3
 34    2   21   16   15    0    1    3
 35    2   21   16   17    0    1    3
 36    2   20   15   14    0    1    3
 37    2   20   15   16    0    1    3
 38    2   22   17   16    0    1    3
 39    2   22   17   18    0    1    3
 40    2    1    7   13    0    1    3
 41    2    7    1    6    0    1    3
 42    2    7    1    2    0    1    3
```

```
   43    2    1    6    4    0    1    3
   44    2    1    2    3    0    1    3
   45    2    1    2    8    0    1    3
   46    2    1    2    9    0    1    3
   47    2    9    2    8    0    1    3
   48    2    1   13   18    0    1    3
   49    2    1   13   14    0    1    3
   50    2    8    2    3    0    1    3
   51    2    9    2    3    0    1    3
   52    2    2    1    6    0    1    3
   53    2    6    1   13    0    1    3
   54    2    2    1   13    0    1    3
   55    2    2    3    4    0    1    3
   56    2    5    4    6    0    1    3
   57    2    5    4    3    0    1    3
   58    2   11    5   12    0    1    3
   59    2   12    5    4    0    1    3
   60    5    8    2    1   13    0    4
   61    5    6    1   13   14    0    4
   62    5    7    1   13   18    0    4
   63    5    2    1    6    4    0    4
   64    5   19   14   13    1    0    4
   65    5    3    2    1    6    0    4
   66    5    3    2    1    7    0    4
   67    5    6    4    5   11    0    4
   68    5    2    1   13   18    0    4
   69    1   19   24    0    0    1    2
   70    2   24   19   14    0    1    3
   5.200     5.000     4.500     5.000     5.200     5.300     5.200
4.500
   5.200     5.300     4.500     5.200     5.300     4.500     5.000
5.000
   5.300     4.500     5.300     5.300     4.500     4.500     5.300
5.000
   0.650     0.650     1.250     0.650     0.650     1.000     0.650
1.250
   1.250     1.250     1.250     0.650     0.650     0.650     0.650
0.650
   0.650     0.650     0.650     1.250     0.650     1.250     0.650
1.250
   1.250     0.650     1.250     1.250     1.250     1.000     1.250
1.000
   1.250     0.750     0.650     0.024     0.024     0.024     0.024
0.024
   0.024     0.024     0.024     0.024     0.830     0.830
  24    1    2
    12.0      12.0      12.0      12.0      12.0      16.0      1.0
1.0
    16.0      16.0      16.0      1.0       14.0      12.0      14.0
12.0
    12.0      12.0      16.0      1.0       16.0      1.0       1.0
1.0
```

```
    13.0      12.0      12.0      12.0      12.0      16.0      1.0
1.0
    16.0      16.0      16.0      1.0       14.0      12.0      14.0
12.0
    12.0      12.0      16.0      1.0       16.0      1.0       1.0
1.0
    12.0      13.0      12.0      12.0      12.0      16.0      1.0
1.0
    16.0      16.0      16.0      1.0       14.0      12.0      14.0
12.0
    12.0      12.0      16.0      1.0       16.0      1.0       1.0
1.0
    12.0      12.0      12.0      12.0      12.0      16.0      1.0
1.0
    16.0      16.0      16.0      1.0       15.0      12.0      14.0
12.0
    12.0      12.0      16.0      1.0       16.0      1.0       1.0
1.0
    12.0      12.0      12.0      12.0      12.0      16.0      2.0
1.0
    16.0      16.0      16.0      1.0       14.0      12.0      14.0
12.0
    12.0      12.0      16.0      1.0       16.0      1.0       1.0
1.0
    12.0      12.0      12.0      12.0      12.0      16.0      1.0
2.0
    16.0      16.0      16.0      2.0       14.0      12.0      14.0
12.0
    12.0      12.0      16.0      1.0       16.0      1.0       1.0
1.0
    12.0      12.0      12.0      12.0      12.0      16.0      1.0
1.0
    16.0      16.0      16.0      2.0       14.0      12.0      14.0
12.0
    12.0      12.0      16.0      1.0       16.0      1.0       1.0
1.0
imidazole BO's adjusted as function of axial BO  O18, C16 BO's set = to
reactant values.  protonation of O2 running in spartan with UFH/3-21G*
   12   70    0    1.1
   12   71    0    0.05
   12   40    0    0.05
   12   54    0    0.05
   12   53    0    0.05
   70   40    0   -0.05
   70   54    0   -0.05
   70   53    0   -0.05
   71   40    0   -0.05
   71   54    0   -0.05
   71   53    0   -0.05

    1    0    3 C-1  0.000       0.0       0.0       1.000
   13    0    3 N-13 1.492      72.296  -268.731     1.076
    6    0    3 O-6  1.445     117.974  -167.279     1.069
```

2	0	3	C-2	1.509	39.621	-86.882	0.938
7	0	3	H-7	1.100	127.129	-9.837	1.000
4	6	3	C-4	1.445	61.266	-125.537	1.209
5	4	3	C-5	1.509	95.283	-191.474	0.998
3	4	3	C-3	1.509	21.350	5.976	0.932
10	3	3	O-10	1.445	63.339	-94.330	1.025
9	2	3	O-9	1.445	111.381	-64.835	1.035
11	5	3	O-11	1.445	57.057	-256.605	0.998
14	13	3	C-14	1.492	25.959	79.176	1.541
18	13	3	C-18	1.492	86.134	-211.542	0.898
19	14	3	O-19	1.445	93.034	-32.510	2.132
15	14	3	N-15	1.492	76.654	-268.653	1.573
16	15	3	C-16	1.492	85.380	-215.455	1.484
20	15	3	H-20	1.008	82.775	24.374	1.280
17	16	3	C-17	1.509	100.097	-150.230	1.199
21	16	3	O-21	1.445	76.340	85.337	2.223
22	17	3	H-22	1.100	85.699	-210.880	1.116
23	18	3	H-23	1.100	100.483	-147.780	1.119
8	2	3	H-8	1.100	38.941	34.957	1.078
12	5	3	H-12	1.100	165.025	-215.967	1.066
24	19	3	H-24	0.958	83.965	39.509	0.874
2	3	0	C-2	1.509			0.942
13	18	0	N-13	1.492			1.455

imidazole BO's adjusted as function of axial BO O18, C16 BO's set = to reactant values. protonation of O_2 running in Gaussian with UHF/6-31G*.

12	70	0	1.1
12	71	0	0.05
12	40	0	0.05
12	54	0	0.05
12	53	0	0.05
70	40	0	-0.05
70	54	0	-0.05
70	53	0	-0.05
71	40	0	-0.05
71	54	0	-0.05
71	53	0	-0.05

1	0	3	C-1	0.000	0.0	0.0	1.000
13	0	3	N-13	1.492	76.893	12.750	0.777
6	0	3	O-6	1.445	110.425	-241.427	1.340
2	0	3	C-2	1.509	37.680	-149.736	0.924
7	0	3	H-7	1.100	134.671	-87.114	1.000
4	6	3	C-4	1.445	68.305	-186.709	1.284
5	4	3	C-5	1.509	57.086	-267.347	0.982
3	4	3	C-3	1.509	59.540	-102.046	0.913
10	3	3	O-10	1.445	126.302	-116.267	1.154
9	2	3	O-9	1.445	82.150	-84.305	1.167
11	5	3	O-11	1.445	40.483	-8.642	1.153
14	13	3	C-14	1.492	77.453	-49.295	1.849
18	13	3	C-18	1.492	94.080	69.381	0.898
19	14	3	O-19	1.445	83.508	-106.241	1.714

15	14	3	N-15	1.492	84.064	10.883	1.779
16	15	3	C-16	1.492	94.933	64.144	1.337
20	15	3	H-20	1.008	76.627	-52.218	1.381
17	16	3	C-17	1.509	100.462	-227.753	1.151
21	16	3	O-21	1.445	83.618	4.624	2.424
22	17	3	H-22	1.100	94.350	70.037	1.142
23	18	3	H-23	1.100	100.629	-224.189	1.119
8	2	3	H-8	1.100	34.116	56.733	1.076
12	5	3	H-12	1.100	125.591	72.579	1.051
24	19	3	H-24	0.958	78.320	-169.786	1.507
2	3	0	C-2	1.509			0.950
13	18	0	N-13	1.492			1.342

imidazole BO's adjusted as function of axial BO O18, C16 BO's set = to reactant values. protonation of O_2 running in spartan UHF/6-31G*.

12	70	0	1.1
12	71	0	0.05
12	40	0	0.05
12	54	0	0.05
12	53	0	0.05
70	40	0	-0.05
70	54	0	-0.05
70	53	0	-0.05
71	40	0	-0.05
71	54	0	-0.05
71	53	0	-0.05

1	0	3	C-1	0.000	0.0	0.0	1.000
13	0	3	N-13	1.492	90.612	78.247	0.777
6	0	3	O-6	1.445	133.317	-164.371	1.339
2	0	3	C-2	1.509	28.381	-138.562	0.925
7	0	3	H-7	1.100	102.980	-28.436	1.000
4	6	3	C-4	1.445	70.279	-136.350	1.282
5	4	3	C-5	1.509	88.865	-206.429	0.981
3	4	3	C-3	1.509	27.118	-41.293	0.914
10	3	3	O-10	1.445	94.787	-50.315	1.154
9	2	3	O-9	1.445	51.209	-17.404	1.168
11	5	3	O-11	1.445	50.315	86.017	1.155
14	13	3	C-14	1.492	59.491	23.732	1.854
18	13	3	C-18	1.492	125.639	-230.869	0.898
19	14	3	O-19	1.445	51.312	-45.727	1.706
15	14	3	N-15	1.492	96.271	72.685	1.784
16	15	3	C-16	1.492	125.999	-237.456	1.335
20	15	3	H-20	1.008	57.429	21.222	1.381
17	16	3	C-17	1.509	117.710	-155.758	1.185
21	16	3	O-21	1.445	92.865	67.503	2.417
22	17	3	H-22	1.100	125.977	-229.821	1.102
23	18	3	H-23	1.100	116.222	-152.604	1.120
8	2	3	H-8	1.100	65.032	-231.523	1.076
12	5	3	H-12	1.100	157.335	-233.650	1.048
24	19	3	H-24	0.958	69.323	-117.069	1.506
2	3	0	C-2	1.509			0.947
13	18	0	N-13	1.492			1.341

Part of the output file:

```
CARTESIAN COORDINATES (BLOCK  1)

 ATOM     1         2         3         4         5         6         7
8         9        10
   X    0.000000 -0.546057 -1.358531 -1.884574 -3.240751 -0.951103
0.942569 -1.154119  0.494017 -0.466365
   Y    0.000000 -0.482058 -1.618586 -1.156559 -0.482491 -0.266072 -
0.510411  0.283011 -0.808077 -2.693778
   Z    0.000000  1.348205  0.898341 -0.468786 -0.438781 -0.931239 -
0.247072  1.803252  2.224284  0.781339
0CARTESIAN COORDINATES (BLOCK  2)

 ATOM    11        12        13        14        15        16        17
18        19        20
   X   -3.165820 -3.488777  0.319310  1.349974  1.739998  1.128383 -
0.048643 -0.462482  2.050027  2.455781
   Y    0.593659 -0.145461  1.534740  1.987856  3.238925  4.197343
3.667329  2.495672  1.269808  3.516875
   Z    0.456342 -1.440853 -0.016745  0.646681  0.502677 -0.323330 -
1.001331 -0.904904  1.449755  0.993194
0CARTESIAN COORDINATES (BLOCK  3)

 ATOM    21        22        23        24
   X    1.579420 -0.607753 -1.311528  1.694456
   Y    5.286405  4.329438  2.055643  0.574033
   Z   -0.382322 -1.630420 -1.375917  1.744650

 ---------------------------------------------------------------------
-------------------------------------------------
 ---------------------------------------------------------------------
-------------------------------------------------
1
1
                                    SUMMARY OF ISOTOPE EFFECTS
                                    ==========================
Mansoureh Rezaei Thymidine Phophorylase expanded SN2 with inversion.
Aug 21, 1998.  This file incorporates the geometry at C5' of uri into
the transition state TS couples reaction coordinate with walden
inversion.30 degrees, protonation of O2 C5' hydroxymethyl geometry of
ino part of TS m.
0ISOTOPE  TEMPERATURE                    COMPLEX
0                          1         2         3
                        Primary C-13

    2       303.0      1.027662  1.030982  1.030905
0                         Secondary C-13

    3       303.0      1.003321  0.999847  0.999859
```

```
0                          primary N-15

    4       303.0       0.999020  1.003322  1.003236
0                          Secondary H-2 1'

    5       303.0       1.180712  1.156540  1.156528
0                          Secondary H-2 2'

    6       303.0       0.976850  0.926047  0.931240
0                          Remote H-2 5'

    7       303.0       0.989100  0.994310  0.998917
1
                SUMMARY OF THE VARIOUS COMPONENTS OF THE ISOTOPE
EFFECT    ( 303.0 DEG.K)
Mansoureh Rezaei Thymidine Phophorylase expanded SN2 with inversion
Aug 21, 1998.  This file incorporates the geometry at C5' of uri into
the ino part of TS m.
0                          Primary C-13

 COMPLEX   TRANS.     ROT.       MMI        EXC         ZPE        EXC.ZPE
VP   VP.EXC.ZPE  VL1/VL2    K1/K2
   1     1.000026  0.998743  0.998769  1.002366    1.026500    1.028928
0.987291  1.015851  1.011626  1.027662
            0.10     -4.61     -4.52      8.66       95.86       104.52
-46.89     57.64     42.36
   2     1.000026  1.000472  1.000498  0.999101    1.031396    1.030469
0.988437  1.018553  1.012202  1.030982
            0.09      1.55      1.63     -2.95      101.32        98.37
-38.13     60.25     39.75
   3     1.000026  1.000491  1.000517  0.999049    1.031352    1.030372
0.988519  1.018542  1.012137  1.030905
            0.09      1.61      1.70     -3.13      101.43        98.30
-37.95     60.36     39.64
                         Secondary C-13

 COMPLEX   TRANS.     ROT.       MMI        EXC         ZPE        EXC.ZPE
VP   VP.EXC.ZPE  VL1/VL2    K1/K2
   1     1.000026  0.999764  0.999790  1.000023    1.003508    1.003531
0.999796  1.003327  0.999994  1.003321
            0.79     -7.11     -6.32      0.69       105.63       106.32
-6.15     100.17     -0.17
   2     1.000026  1.000598  1.000624  0.998743    1.000481    0.999223
1.000589  0.999812  1.000035  0.999847
           -17.13   -389.90   -407.03    820.34     -313.32       507.03
-384.35    122.67    -22.67
   3     1.000026  1.000600  1.000627  0.998742    1.000492    0.999232
1.000590  0.999822  1.000037  0.999859
           -18.59   -424.87   -443.45    891.27     -347.82       543.45
-417.20    126.25    -26.25
0                          primary N-15
```

```
 COMPLEX   TRANS.     ROT.      MMI       EXC        ZPE       EXC.ZPE
VP   VP.EXC.ZPE  VL1/VL2    K1/K2
   1     1.000026  0.998829  0.998855  1.007107    0.993107    1.000165
0.994943  0.995107  1.003932  0.999020
           -2.68    119.47    116.79   -722.20      705.41      -16.79
516.99    500.20   -400.20
   2     1.000026  1.000141  1.000167  0.999213    1.003945    1.003155
0.995644  0.998785  1.004542  1.003322
            0.79      4.24      5.03    -23.74      118.71       94.97
-131.61    -36.64    136.64
   3     1.000026  1.000147  1.000173  0.999301    1.003764    1.003062
0.995598  0.998647  1.004595  1.003236
            0.81      4.54      5.35    -21.65      116.30       94.65
-136.57    -41.92    141.92
0                        Secondary H-2 1'

 COMPLEX   TRANS.     ROT.      MMI       EXC        ZPE       EXC.ZPE
VP   VP.EXC.ZPE  VL1/VL2    K1/K2
   1     1.000026  0.997433  0.997459  1.004120    1.178863    1.183719
0.973464  1.152308  1.024649  1.180712
            0.02     -1.55     -1.54      2.48       99.05      101.54
-16.25     85.32     14.68
   2     1.000026  1.000923  1.000949  0.997843    1.157941    1.155443
0.973499  1.124823  1.028197  1.156540
            0.02      0.64      0.65     -1.49      100.83       99.35
-18.52     80.86     19.14
   3     1.000026  1.000964  1.000991  0.997689    1.158059    1.155383
0.973677  1.124970  1.028052  1.156528
            0.02      0.66      0.68     -1.59      100.91       99.32
-18.40     80.96     19.04
0                        Secondary H-2 2'

 COMPLEX   TRANS.     ROT.      MMI       EXC        ZPE       EXC.ZPE
VP   VP.EXC.ZPE  VL1/VL2    K1/K2
   1     1.000052  0.999238  0.999290  1.001089    0.976481    0.977544
1.002442  0.979931  0.996855  0.976850
           -0.22      3.26      3.03     -4.65      101.61       96.97
-10.42     86.55     13.45
   2     1.000052  1.000729  1.000781  1.000302    0.925045    0.925324
1.003214  0.928299  0.997575  0.926047
           -0.07     -0.95     -1.02     -0.39      101.41      101.02
-4.18      96.84      3.16
   3     1.000052  1.000679  1.000731  1.000018    0.930543    0.930560
1.003198  0.933536  0.997541  0.931240
           -0.07     -0.95     -1.03     -0.03      101.05      101.03
-4.48      96.54      3.46
0                        Remote H-2 5'

 COMPLEX   TRANS.     ROT.      MMI       EXC        ZPE       EXC.ZPE
VP   VP.EXC.ZPE  VL1/VL2    K1/K2
   1     1.000026  0.999624  0.999650  1.001667    0.987799    0.989446
1.001535  0.990965  0.998118  0.989100
```

```
          -0.24      3.43      3.19    -15.20      112.01       96.81
-14.00     82.81     17.19
   2     1.000026  0.999197  0.999223  0.999707    0.995374    0.995083
1.001289  0.996366  0.997936  0.994310
          -0.46      14.08     13.62      5.13       81.25       86.38
-22.58     63.79     36.21
   3     1.000026  0.999168  0.999195  0.999503    1.000219    0.999722
1.001273  1.000995  0.997924  0.998917
          -2.42      76.75     74.32     45.86      -20.19       25.68
-117.42    -91.74    191.74
1
SUMMARY OF THE EFFECTS OF TUNNELLING ON THE ISOTOPE EFFECT    ( 303.0
DEG.K)
Mansoureh Rezaei Thymidine Phophorylase expanded sn2 with inversion
Aug 21, 1998.  This file incorporates the geometry at C5' of uri into
the part of TS m.
IMAGINARY FREQUENCIES FOR NORMAL ISOTOPIC COMPLEXES (1/CM)0

     COMPLEX0-            1         2         3
                         -325.10   -261.17   -260.69
0                       Primary C-13

     COMPLEX0-            1         2         3
 IMAG.FREQ.(/CM)         -321.44   -258.21   -257.76
 K1/K2(UNCORR.)         1.027662  1.030982  1.030905
 K1/K2(WIGNER)          1.029743  1.032382  1.032292
 K1/K2(BELL)            1.030042  1.032510  1.032418
0                       Secondary C-13

     COMPLEX0-            1         2         3
 IMAG.FREQ.(/CM)         -324.84   -260.89   -260.41
 K1/K2(UNCORR.)         1.003321  0.999847  0.999859
 K1/K2(WIGNER)          1.003464  0.999977  0.999989
 K1/K2(BELL)            1.003485  0.999989  1.000001
0                       primary N-15

     COMPLEX0-            1         2         3
 IMAG.FREQ.(/CM)         -323.28   -260.14   -259.66
 K1/K2(UNCORR.)         0.999020  1.003322  1.003236
 K1/K2(WIGNER)          1.000026  1.003798  1.003711
 K1/K2(BELL)            1.000171  1.003841  1.003754
0                       Secondary H-2 1'

     COMPLEX0-            1         2         3
 IMAG.FREQ.(/CM)         -317.50   -254.44   -254.01
 0                       Secondary H-2 2'

     COMPLEX0-            1         2         3
 IMAG.FREQ.(/CM)         -324.71   -260.75   -260.28
 K1/K2(UNCORR.)         0.976850  0.926047  0.931240
 K1/K2(WIGNER)          0.977060  0.926227  0.931417
 K1/K2(BELL)            0.977090  0.926244  0.931434
0                       Remote H-2 5'
```

COMPLEX0-	1	2	3
IMAG.FREQ.(/CM)	-325.08	-261.16	-260.68
K1/K2(UNCORR.)	0.989100	0.994310	0.998917
K1/K2(WIGNER)	0.989108	0.994313	0.998920
K1/K2(BELL)	0.989109	0.994313	0.998920
K1/K2(UNCORR.)	1.180712	1.156540	1.156528
K1/K2(WIGNER)	1.185655	1.160095	1.160049
K1/K2(BELL)	1.186359	1.160415	1.160366

1

LITERATURE CITED

1. Leer, J.C., Hammer-Jerpersoen, K., and Schwartz, M. *Eur. J. Biochemistry* **1977**,*75*, 217-224.
2. Kraut, A., and Yamada, E.W. *J. Biol. Chem.* **1971**,*246*, 2021-2030.
3. Moghaddam, A. and Bicknell, R. *J. Biochemistry* **1992**,*31*, 12142-12146.
4. Shaw, T., Smillie, R.H., and MacPhee, D.G. *Cancer Res.* **1988**, *200*, 99-116.
5. Jeffery, C.J. Moonlighting Proteins, *Trends Biochem. Soc.* ***1999***, *24*, 8-11.
6. Folkman,J. *J. National Cancer Institute* **1996**, *88*.
7. Desgranges, C., Razaka, G., Rabaud, M., and Bricaud, H. *Biochim. Biophys. Acta*, **1981**, *654*, 211-218.
8. Schwartz, M. *Eur. J. Biochem.* **1971**, *21*, 191-198.
9. Schwartz, M. *Methods Enzymol.* 1978, 51, pp 442-445.
10. Walter, Mark R., Cook, William J., Cole, Brent L., et al. *J. Biol. Chem.* **1990**, *256*, 14016-14022.
11. Brown, S.N and Bicknell, R. *J. Biochemistry* **1998**, *334*, 1-8.
12. Pugmire, M.J., Ealick, S.E. *Structure* **1998**, *6*, 1467-1479.

13. Ealicks, S.E., Rule, S.A., Carter, D.C., Grennthough, T.J., Babu, Y.S., Cook, W.J., Habash, J., Well, J.R., Stoechler, J.D., Parks, R.E., Chen, S., and Bugg, C.E. *J. Biol. Chem.* **1999**, *265*, 1820-1821.

14. Mao, C., Cook, W.Y., Zhou, M., Federov, A., Almo, S.C., and Ealick, S.E. *J. Biochemistry* **1998**, *37*, 7135-7146.

15. Ittzsch, M.H., el-Kouri, M.H. and Cha, S. *J. Biochemistry* **1985**, *24*, 6799-6807.

16. Hori, A., Sasada, R., Hatsutani, E., et al. *Cancer Res.* **1991**, *51*, 6180-6184.

17. Reynolds, L.P., Killilea, S.D., Redmer, D.A. *FASEB J.* **1992**, *6*, 886-892.

18. Asai, K., Nakanishi, K., Isoabe, L., et al. *J. Biol. Chem.* **1992**, *267*, 20311-20316.

19. Furukawa, T., Yoshimura, A., Sumizawa, T., et al. *Nature*, **1992**, *356*, 668.

20. Folkman, J. and Kiagsbrun, M. *J. Science* **1987**, *235*, 442-447.

21. Folkman, J. *J. Natl. Cancer Inst.* **1990**, *82*, 4-6.

22. Balzarini, J., Esteban, A., Esnouf, R., Liekens S., Neyts, J., Camarasa, M. *FEBS Lett.* **1998**, *438* (1,2), 91-95.

23. Balzarini, J., Esteban, A., Esnouf, R., Liekens S., Neyts, J., Camarasa, M. *J. Med. Chem.* **2000**, *43* (5), 971-983.

24. Liotta, L., Kleinerman, J. and Saidel, G. *Cancer Res.* **1974**, *34*, 1587-1590.

25. Pauly, J.L., Schuller M.G., Zelcer A.A., et al. *J. Natl. Cancer Inst.* **1977**, *58*, 1587-1590.

26. Herlyn, M., Clark, W.H., Rodeck, U., Mancianti, M.L., Jambrosic, J. and Koprowski, H. *Lab. Invest.* **1987**, *56*, 461-474.

27. Weidner, N., Semple, J.P., Wetch, W.R. et al. *N. Engl. J. Med.* **1991**, *324*, 1-8.

28. Ishidawa, F., Miyazono, K., Hellman, U., et al. *Nature* **1984**, *338*, 557-562.

29. Yoshimura, A., Kuwarzuru, Y., Frukawa, T., et al. *Biochim. Biophys. Acta*, **1990**, *1034*, 107-113.

30. Weidner, N., Folkman, J., Pozza, F., et al. *J. Natl. Cancer Inst.* **1992**, *84*, 1875-1887.

31. Takebayashi, Y., Miyadera, K., Akiyam, S., Hokita, S., Yamada, K., Akiba, S., Yamada, Y., Sumizaw, T., Aikou, T. *Cancer Res.* **1996**, *87*, 288-295.

32. Kouni, M.H., Kouni, M.M., and Naguib, N.F. *Cancer Res.* **1993**, *53*, 3687-3693.

33. Sherwood, D. *Crystals, X-ray and Proteins*; John Wiley & Sons: New York, 1976.

34. Schramm, V.L., Horenstein, B.A., and Kline, P.C. *J. Biol. Chem.* **1994**, *269*, 18259-18262.

35. Weiner, D.B., and Williams, W.B. *Chemical and Structural Approaches to Rational Drug Design, III Series: Pharmacology & Toxicology;* CRC Press, Inc.: Boca Raton, FL., 1995; pp 167-170.

36. Parkin, D.W., and Schramm, V.L. *J. Biochemistry* **1987**, *26*, 913-920.

37. Merkler, D.J., Kline, P.C., Weiss, P. and Schramm, V.L. *J. Biochemistry* **1993**, *32*, 12993-13001.

38. Kline, P.C., and Schramm, V.L. *J. Biochemistry* **1993**, *32*, 13212-13219.

39. Horenstein, B.A., Parkin, D.W., Estupinan, B., and Schramm, V.L. *J. Biochemistry* **1991**, *30*, 10788-10795.

40. Boutellier, M., Horenstein, B.A., Semenyaka, A., Schramm, V.L., and Ganem, B. *J. Biochemistry* **1994**, *33*, 3994-4000.

41. Buddenbaum, E.W., and Shiner, J.V. *J. Am. Chem.* Soc. **1976**, *54*, 1-32.

42. Sandler, M., Smith, J.H. *Design Of Enzyme Inhibitors As Drugs*; Oxford University Press Inc.: New York, 1994; p 615.

43. Raaen, V., Ropp G., and Raaen, H.P. *Carbon-14, McGraw-Hill Series In Advanced Chemistry*; 1968; pp 541, 47-51, 319-322.

44. Bigeleisen, J. *J. Chem. Phys.* **1949**, *17*, 675.

45. Yergey L. A., Edmonds, G.C., Lewis S.A., and Vestal L.M. *Liquid Chromatography/Mass Spectrometry Techniques And Applications*; Plenum Press: New York, 1990; pp 89-91.

46. Sims, L.B., Burton, G.W., and Lewis, D.E. BEBOVIB-IV Program **1977**. *Quantum Chemistry Program Exchange*, No. 337.

47. Sims, L.B. and Lewis, S.E. *Isot. Org. Chem.* **1984**, *6*, 161-259.

48. Kirch, J.F. *J. Am. Chem. Soc.* **1976**, *20*, 100-120.

49. Blakeney, A.B., Harris, P.J., Henry, R.J., and Bruce, A. *Carbohydr. Res.* **1983**, *113*, 291-299.

50. Cook, G., and Greenberg, M. *J. Org. Chem.* **1994**, *59*, 4704-4706.

51. Kline, P.C., and Serianni, A. *J. Am. Chem. Soc.* **1990**, *112*, 7323-7381.

52. Baker, D. and Hasker, T. *J. Med. Chem.* **1975**, *18*, 1041-1044.

53. Roberts, L. John and Poulter, C. Dale *J. Org. Chem.* **1978**, *43*, 1547-1550.

54. Waller, M.R., Cook, W.J., Cole, L.B., Short, S.A., Koszalka, G.W., Krenitsky, T.A., and Ealick, S.E. *J. Biol. Chem.* **1990**, *265*, 14016-14022.

55. Krenitsky, T.A., Koszalka, G.W., and Tuttle, J.V. *J. Biochem.* **1981**, *30*, 3615-3621.

56. Krenitsky, T.A., and Tuttle, J.V. *J. Biochim. Biophys. Acta*, **1982**, *703*, 247-249.

57. Miwa, N., Ayako, H., Kazushige, M., Takehisa, M., Takashi, Y., and Hideo, I. *Biol. Pharm. Bull.* **1996**, *19*, 1407-1411.

58. Matsushita, S., Nitanda, T., Furudawa, T., Sumizawa, T., Tani, A., Nishimoto, K., Akiba, S., Miyadera, K.,

Fukushima, M., Yamada, Y., Yoshida, H., Kanzaki, T., Akiyama, S. *Cancer Res.* **1999**, *59*, 1911-1916.

59. Focher, F., Ubiali, D., Pregnolato, M., Zhi, C., Gambino, J., Wright, G., Spadari, S. *J. Med. Chem.* **2000**, *43*, 2601-2607.

60. Gardner, H. *The Disciplined Mind*; Rockefeller Center: New York, 1999.

61. Armstrong, T. *7 Kinds of Smart*. Plume-Penguin: New York, 1993.

62. Martin, N.H. *J. Chem. Ed.* **1998**, *2*, 241-245.

63. Alexandria, V. *Multiple Intelligence in the Classroom;* Association for Supervision and Curriculum Development: New York, 1994.

64. Gardner, H. *Multiple Intelligences for the 21st Century;* Rockefeller Center: New York, 1999.

65. Gardner, H. *Multiple Intelligences*: The Theory In Practice; Basic Books: New York, 1993.

66. Hehre, N.J., Shusterman, A.J., Nelson, J.E. *The Molecular Modeling Workbook for Organic Chemistry;* Wavefunction, Inc.: CA, 1998.